Remost Sensing Assessment of Surface Oil Transport and Fate during Spills in the Gulf of Mexico

WAMOST
(Weathering and Advection Model for Oil Spill Tracking)

BOEM Contract M12PC00003

Project Tasks & Scientific Personnel

- Task 1: Project management
  - Ian MacDonald, FSU
- Task 2: Surface Oil Distribution from Remote Sensing
  - Chuanmin Hu, USF (Optical Remote Sensing)
  - Oscar Garcia. FSU (SAR)
  - Samira Daneshgar Asl, FSU (SAR)
- Task 3: Oil Transport Chemical Modeling Model
  - Mark Reed, SINTEF
  - Jøgen Skancke, SINTEF
- Task 4: Ocean and Wind Forcing
  - Dmitry Dukhovskoy, FSU COAPS
  - Steve Morey, FSU COAPS
- Task 5: Mixing Processes and Wind Forcing
  - Mark Bourassa, FSU COAPS

Peer-Reviewed Publications (to date)

1. Clark M, Heath N, Bourassa MA. 2015. Quantification of Stokes drift as a mechanism for surface oil advection in the Gulf of Mexico. J Geophys Res. (accepted, pending minor revisions)
2. Daneshgar Asl S, Dukhovskoy DS, Bourassa M, MacDonald IR (2017) Hindcast modeling of oil slick persistence from natural seeps. Remote Sensing of Environment 189:96-107
3. Dukhovskoy DS, Leben RR, Chassignet EP, Hall C, Morey SL, Nedbor-Gross R. 2015. Characterization of the uncertainty of Loop Current metrics using a multidecadal numerical simulation and altimeter observations. Deep-Sea Res Pt I. 100: 140-158
4. Dukhovskoy DS, Ubnoske J, Blanchard-Wrigglesworth E, Hiester HR, Proshutinsky A. 2015. Skill metrics for evaluation and comparison of sea ice models. J Geophys Res. 120*,* 5910–5931
5. Garcia-Pineda O, MacDonald I, Hu C, Svejkovsky J, Hess M, Dukhovskoy D, Morey SL. 2013. Detection of floating oil anomalies from the Deepwater Horizon oil spill with synthetic aperture radar. Oceanography. 26(2): 124-137.
6. Garcia-Pineda, O, MacDonald IR, Li X, Jackson CR, Pichel WG. 2013. Oil spill mapping and measurement in the Gulf of Mexico with Textural Classifier Neural Network Algorithm (TCNNA). IEEE J Sel Top Appl Earth Obs Remote Sens. PP(99): 2517-2525.
7. Garcia-Pineda OG, MacDonald IR, Shedd W. 2014. Analysis of oil volume fluxes of hydrocarbon seep formations on the Green Canyon and Mississippi Canyon: a study using 3D-seismic attributes in combination with satellite and acoustic data. SPE Reservoir Eval Eng, 17(4): 430-435
8. GRIIDC: Gulf of Mexico Research Initiative Information and Data Cooperative Database. Corpus Christi (TX). Neural network analysis determination of oil slick distribution and thickness from satellite Synthetic Aperture Radar, April 24 - August 3, 2010 [revised 2016 Jan 21; accessed 2016 Jan 21] https://data.gulfresearchinitiative.org/data/R1.x132.137:0045/.
9. Hiester HR, Morey SL, Dukhovskoy DS, Chassignet EP, Kourafalou VH, Hu C. 2016. A topological approach for quantitative comparisons of ocean model fields to satellite ocean color data. Methods Oceanography, In Review.
10. Hu C, Chen S, Wang M, Murch B, Taylor J. 2015. Detecting surface oil slicks using VIIRS nighttime imagery under moon glint: a case study in the Gulf of Mexico. Remote Sens Lett. 6:295-301.
11. Hu C, Feng L, Holmes J, Swayze GA, Leifer I, Melton C, Garcia O, MacDonald I, Hess M, Muller-Karger F, Graettinger G, Green R. 2016. Remote sensing estimation of surface oil volume during the 2010 Deepwater Horizon oil blowout in the Gulf of Mexico: Scaling up AVIRIS observation with MODIS measurements. Int J Remote Sens. Submitted
12. Lu Y, Sun S, Zhang M, Murch B, Hu C. 2016. Refinement of the critical angle calculation for the contrast reversal of oil slicks under sunglint. J Geophys Res Oceans. 121(1)*:* 148–161
13. MacDonald IR. 2013. Tracking Recovery from Deepwater Horizon. Sea Tech. 54(5): 23-30.
14. MacDonald IR, Garcia-Pineda OM, Beet A, Daneshgar Asl S, Feng L, French McCay DP, Graettinger G, Holmes J, Hu C, Leifer I, Mueller-Karger F, Solow AR, Swayze G. 2015. Natural and unnatural oil slicks in the Gulf of Mexico. J Geophys Res Oceans. 120(12): 8364-8380.
15. MacDonald, I.R., Kammen DM, Fan M. 2014. Science in the aftermath: investigations of the DWH hydrocarbon discharge. Environ Res Lett. 9(12): 125006.
16. Özgökmen TM, Chassignet EP, Dawson C, Dukhovskoy D, Jacobs G, Ledwell J, Garcia-Pineda O, MacDonald I, Morey SL, Olascoaga M, Poje AC, Reed M, Skancke J. 2016. Over what area did the oil and gas spread during the 2010 Deepwater Horizon oil spill? Oceanography. In Review.
17. Sun S, Hu C. 2016. Sun glint requirement for the remote detection of surface oil films. Geophys Res Lett. 43*:* 309–316.
18. Sun S, Hu C, Feng L, Swayze GA, Holmes J, Graettinger, MacDonald I, Garcia O, Leifer I. 2016) Oil slick morphology derived from AVIRIS measurements of the Deepwater Horizon oil spill: Implications for spatial resolution requirements of remote sensors. Mar Pollut Bull. 103(102): 276–285.
19. Sun S, Hu C, Tunnell Jr. JW. 2015. Surface oil footprint and trajectory of the Ixtoc-I oil spill determined from Landsat/MSS and CZCS observations. Mar Pollut Bull. 101:632-641.
20. Wang M, Hu C. 2015. Extracting oil slick features from VIIRS nighttime imagery using a Gaussian filter and morphological constraints. IEEE Geosci Remote Sens Lett. 12(10): 2051-2055.

Task 1: Project Integration

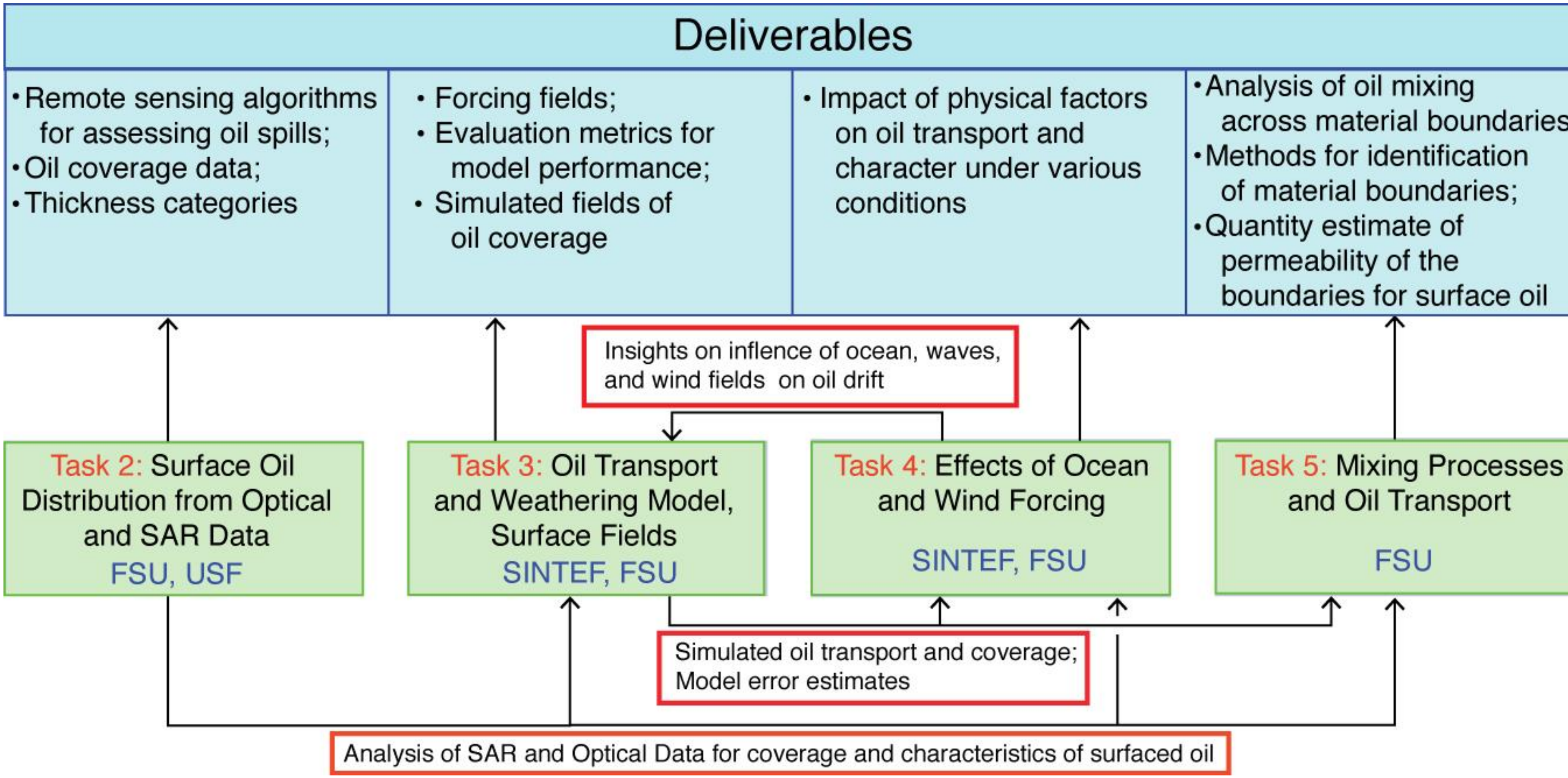

Task 2: Characterize Surface Oil Distributions Using SAR and Optical Remote Sensing

Distribution of DWH surface oil from satellite remote sensing

From SAR (MacDonald et al., unpublished)

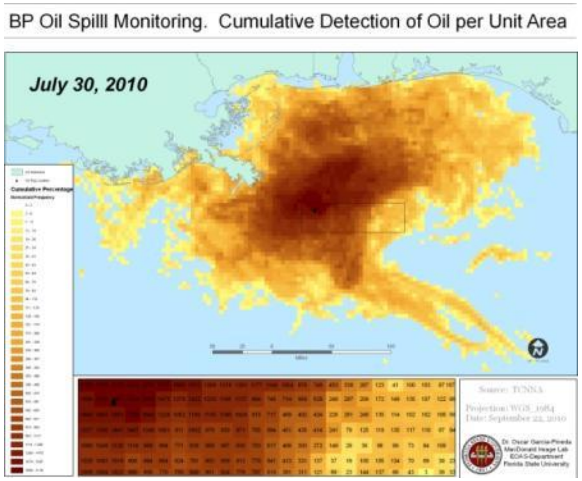

From MODIS/MERIS (Hu et al., 2011)

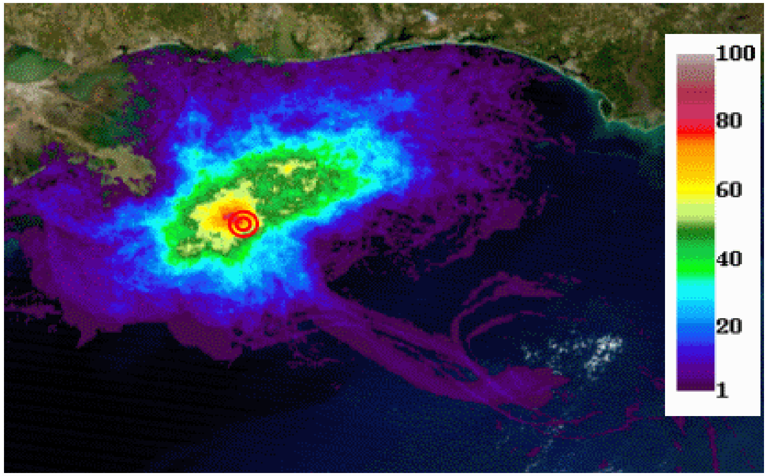

Calibration of surface oil thickness from AVIRIS (below)

Approach:

1. Spectral analysis in the visible, NIR, and shortwave NIR
2. Scaling-up from AVIRIS to MODIS/MERIS

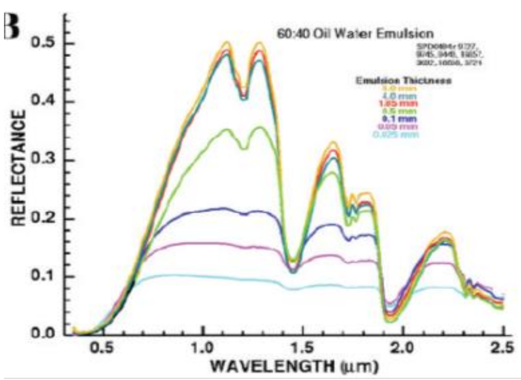

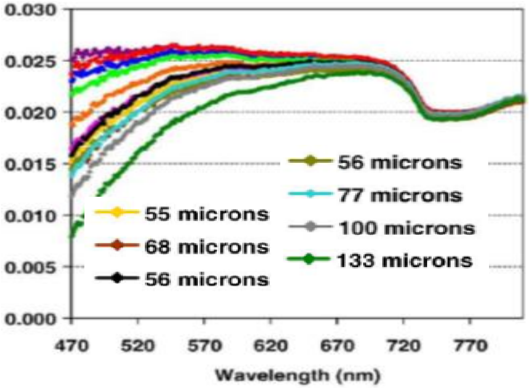

USF UNIVERSITY OF SOUTH FLORIDA

SINTEF

Task 2a: Characterize Surface Oil Distributions Using Optical Remote Sensing

Top: Oil slicks detected by VIIRS but not by MODIST

Bottom: Oil slicks detected by MODISA but not by VIIRS

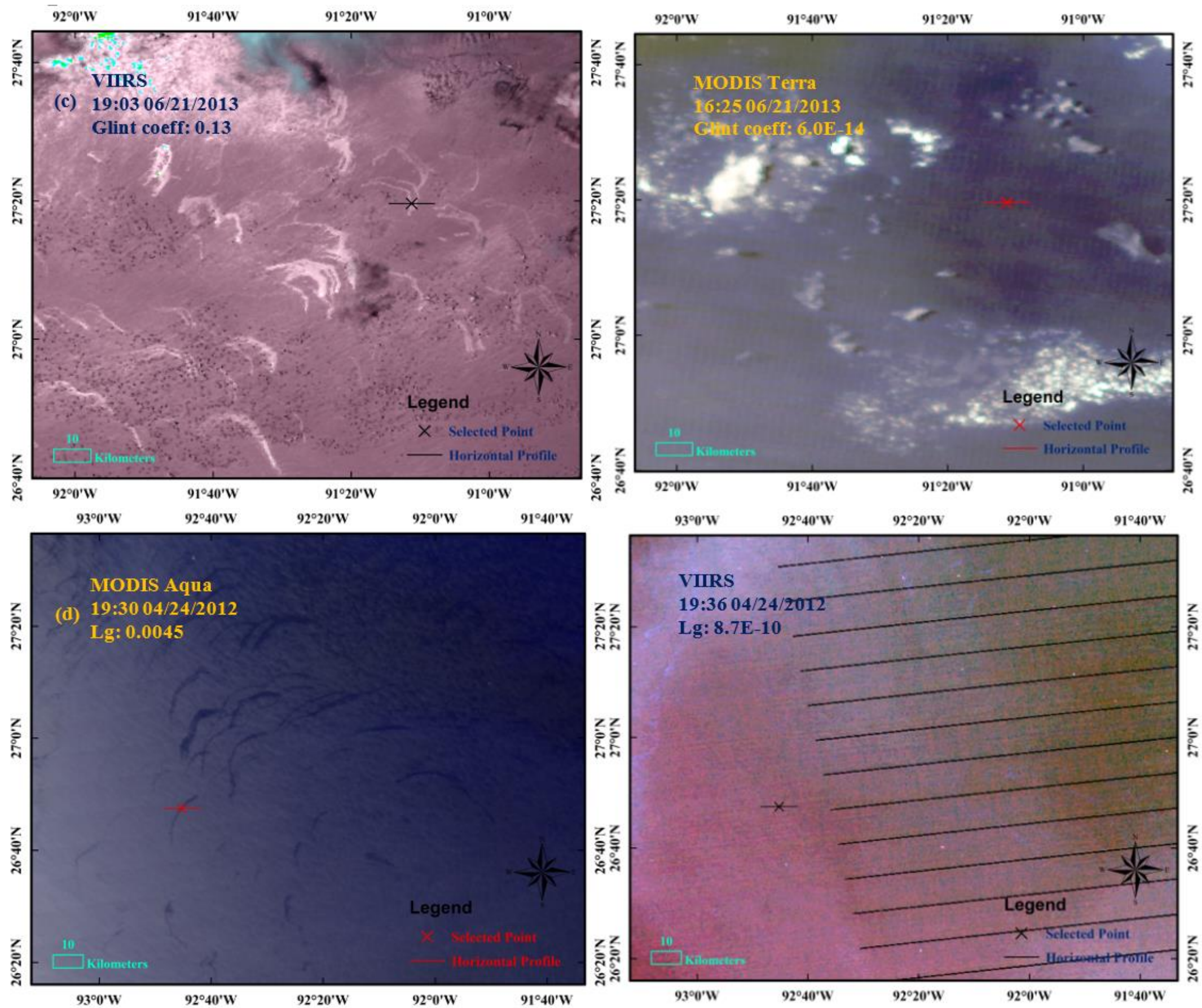

- Sun glint strength determines whether thin oil can be observed or not

  $> 10^{-5}$ sr^{-1}: yes

  $< 10^{-6}$ sr^{-1}: no

  (Sun and Hu, 2016)

Task 2a: Characterize Surface Oil Distributions Using Optical Remote Sensing

Surface oil volume maps derived from MODIS after using histogram-based AVIRIS calibration

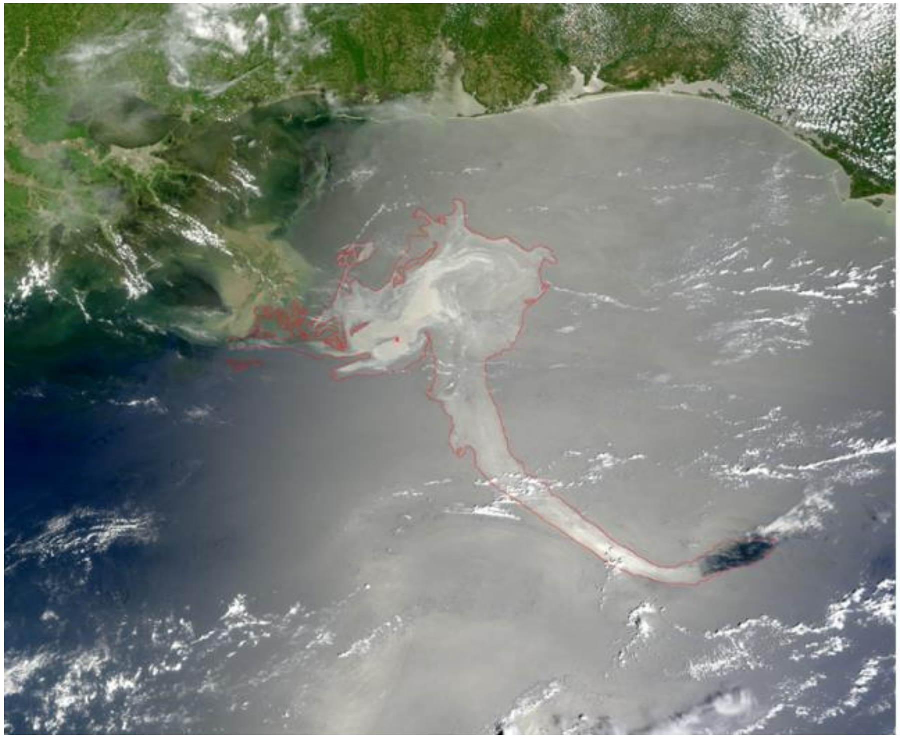

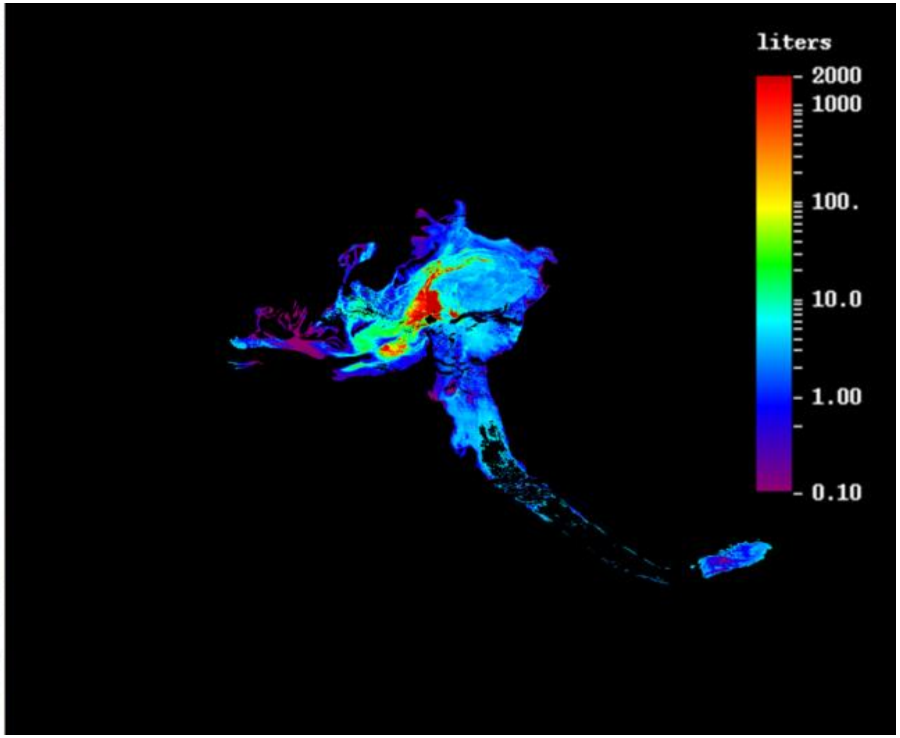

Color legend shows oil volume in liters per MODIS 250-m pixel
Example showing the case for May 17, 2010. 18 other cases are available
(Hu et al., 2016, submitted)

Task 2a: Characterize Surface Oil Distributions Using Optical Remote Sensing

Surface oil thickness classes derived from MODIS after using histogram-based AVIRIS calibration

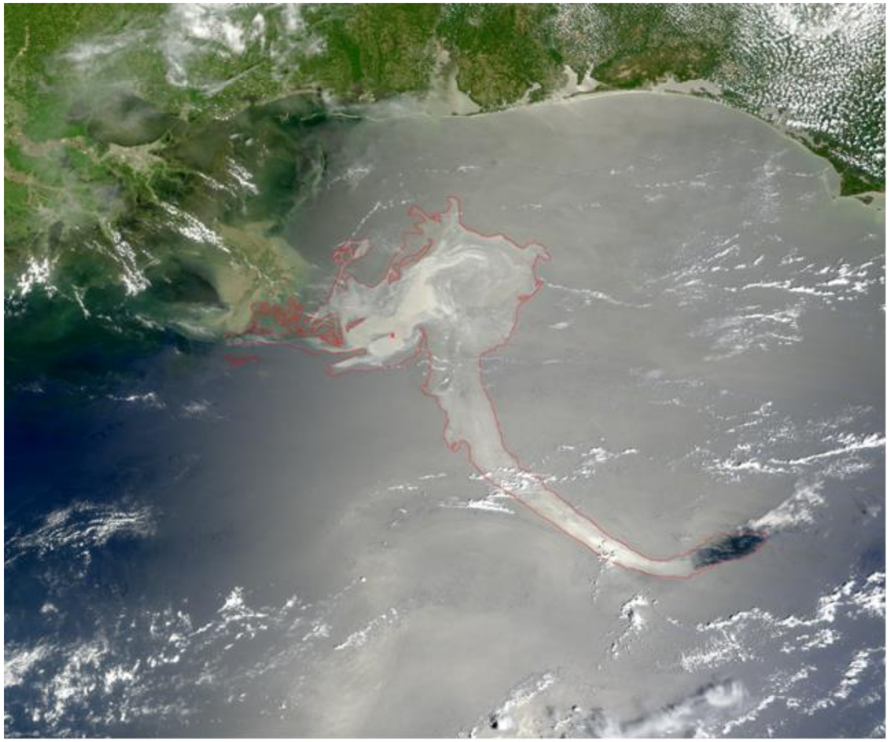

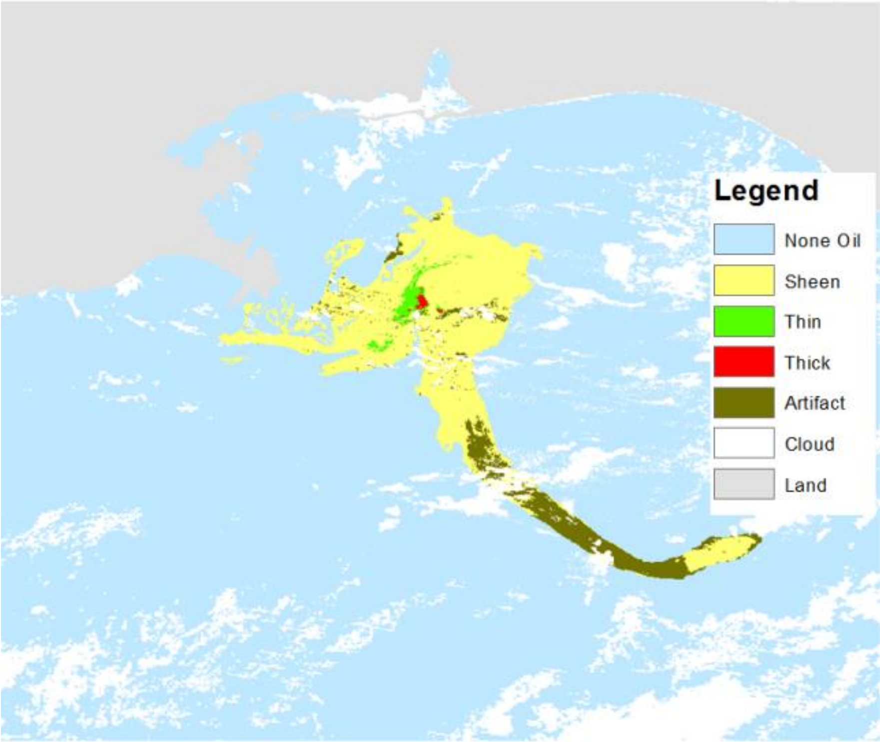

Color legend shows different oil thickness classes and other image features
Example showing the case for May 17, 2010. 18 other cases are available
(Hu et al., 2016, submitted)

Task 2a: Characterize Surface Oil Distributions Using Optical Remote Sensing

Surface oil probability maps

0.1 means that 10% of that location is covered by oil of that thickness

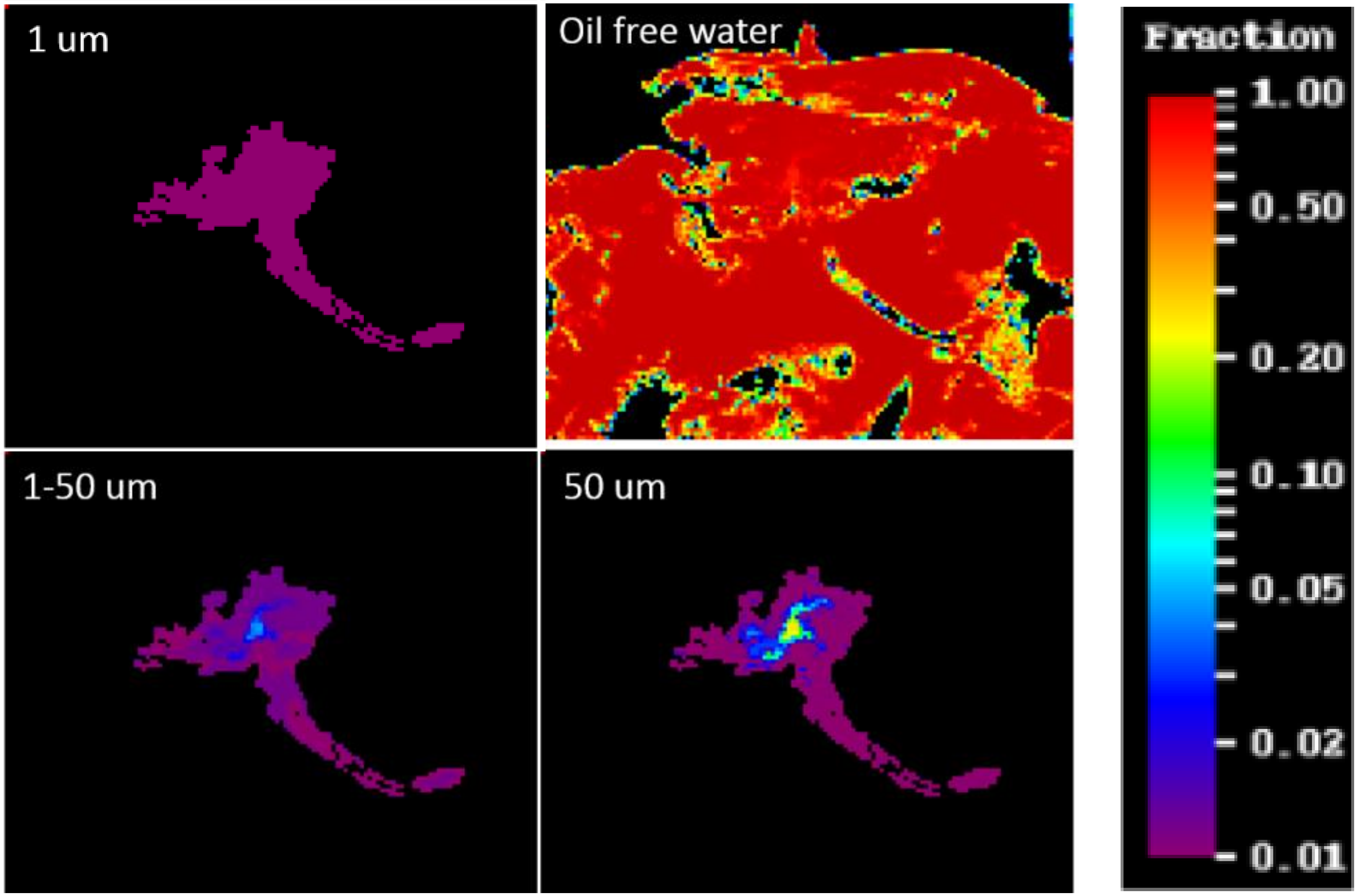

Task 2a: Characterize Surface Oil Distributions Using Optical Remote Sensing

- Oil slick morphology characterized for different oil thickness classes derived from AVIRIS measurements of the DwH. (Sun et al. 2015).
- Thickness estimates obtained by processing AVIRIS images from a limited survey of DwH suggested a median thickness of 70 µm for emulsified oil (Sun, Hu et al. 2015).
- The DwH SAR data set was subsequently used to quantify “thin” (1 µm) and “thick” (70 µm) oil.

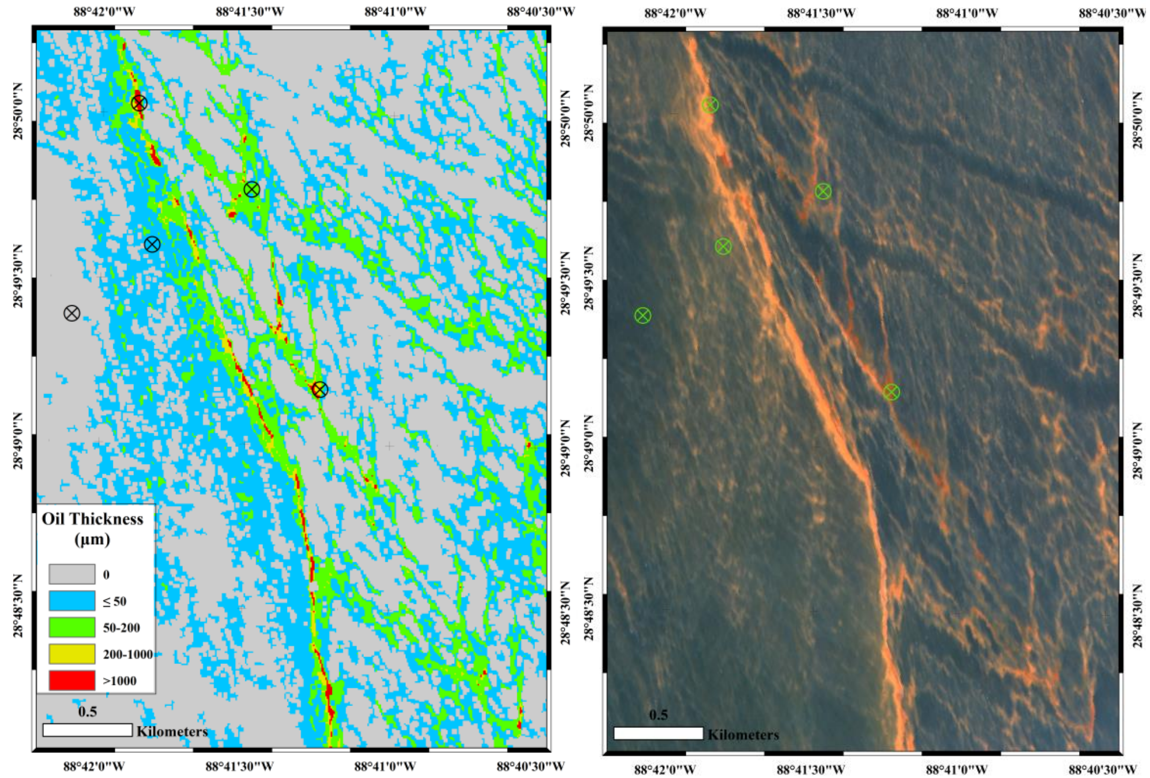

AVIRIS-derived oil thickness (left) and Red-Green-Blue true color maps (from Clark et al., 2010)

Task 2a: Characterize Surface Oil Distributions Using Synthetic Aperture Radar

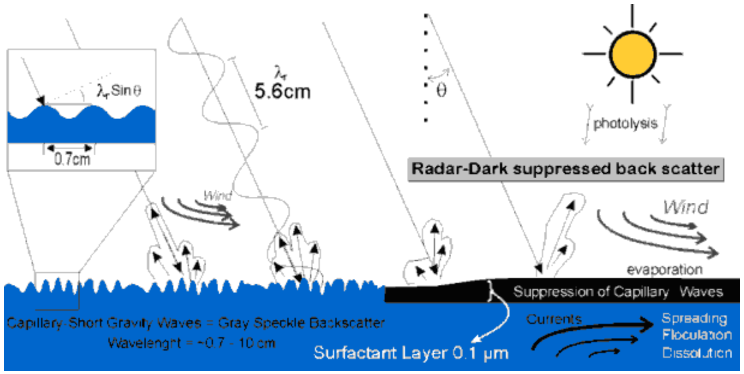

- Satellite SAR image processing was performed using TCNNA algorithm (Garcia-Pineda, Zimmer et al. 2009, Garcia-Pineda, MacDonald et al. 2010)
- TCNNA is an in-house developed algorithm which employs satellite and meteorological variables, and textural analysis to extract oil features from RADAR images.
- Each SAR pixel is classified as feature or non-feature and to reproduce, pixel by pixel, classifications an expert human analyst would evaluate whether a given group of pixels belongs to a feature.

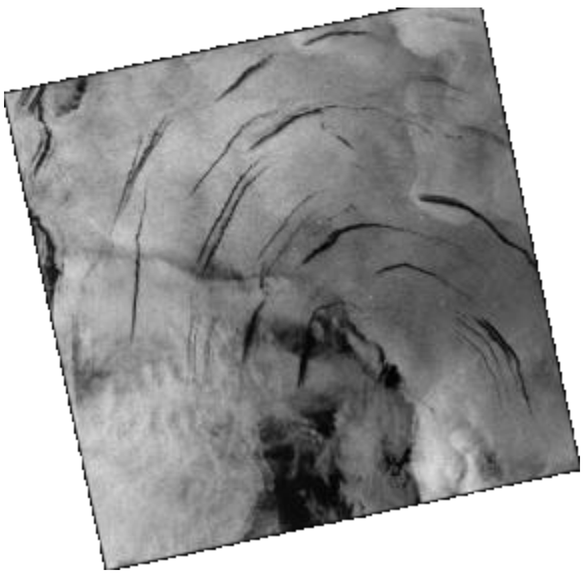

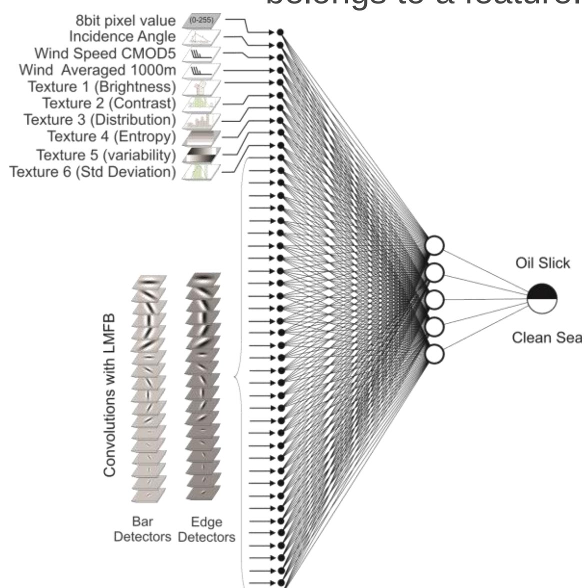

For WAMOST, additional routines were developed to output multiple values corresponding to apparent oil thickness categories.

Mapping Surface Oil with SAR— ~950 Natural Seep Zones

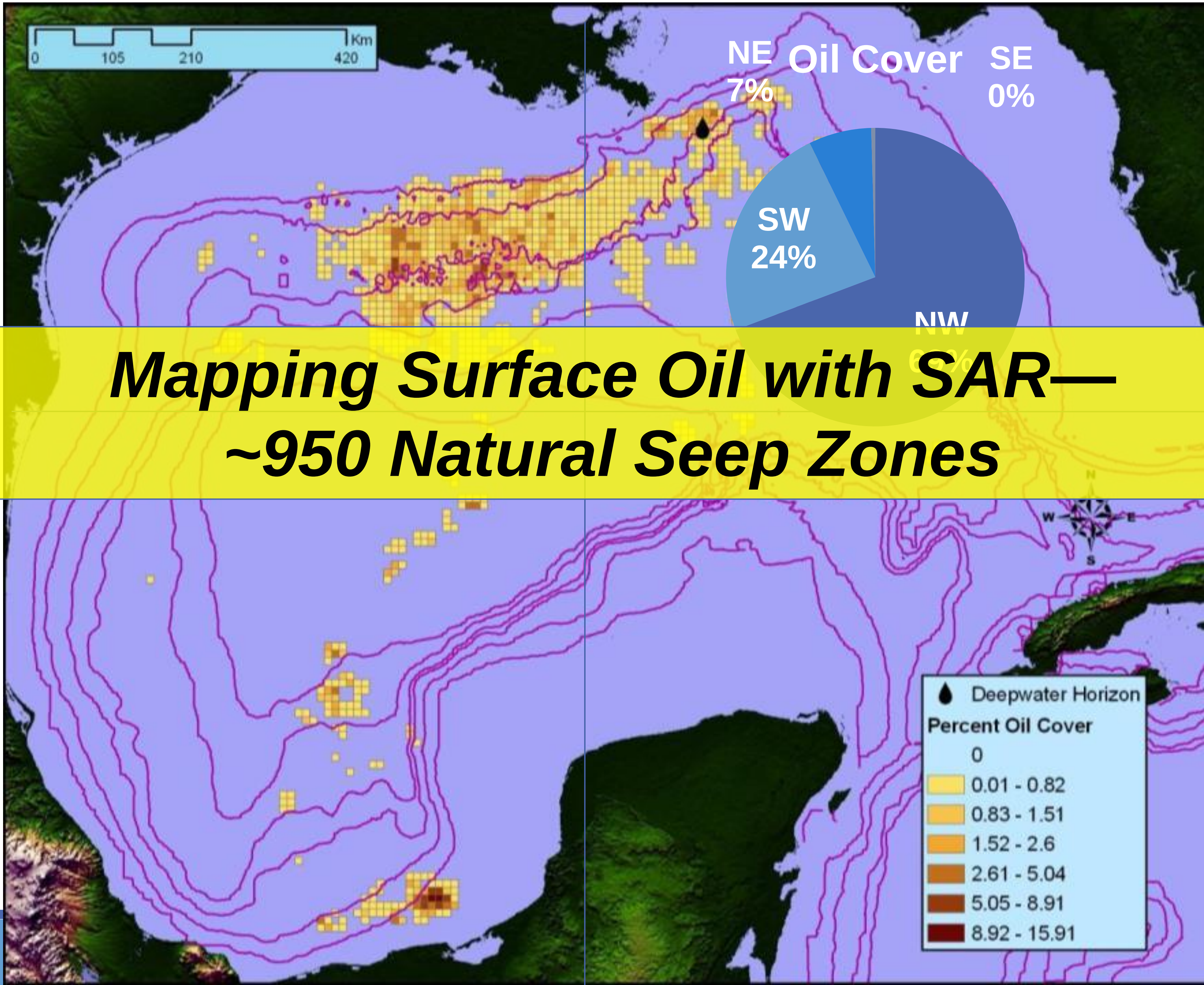

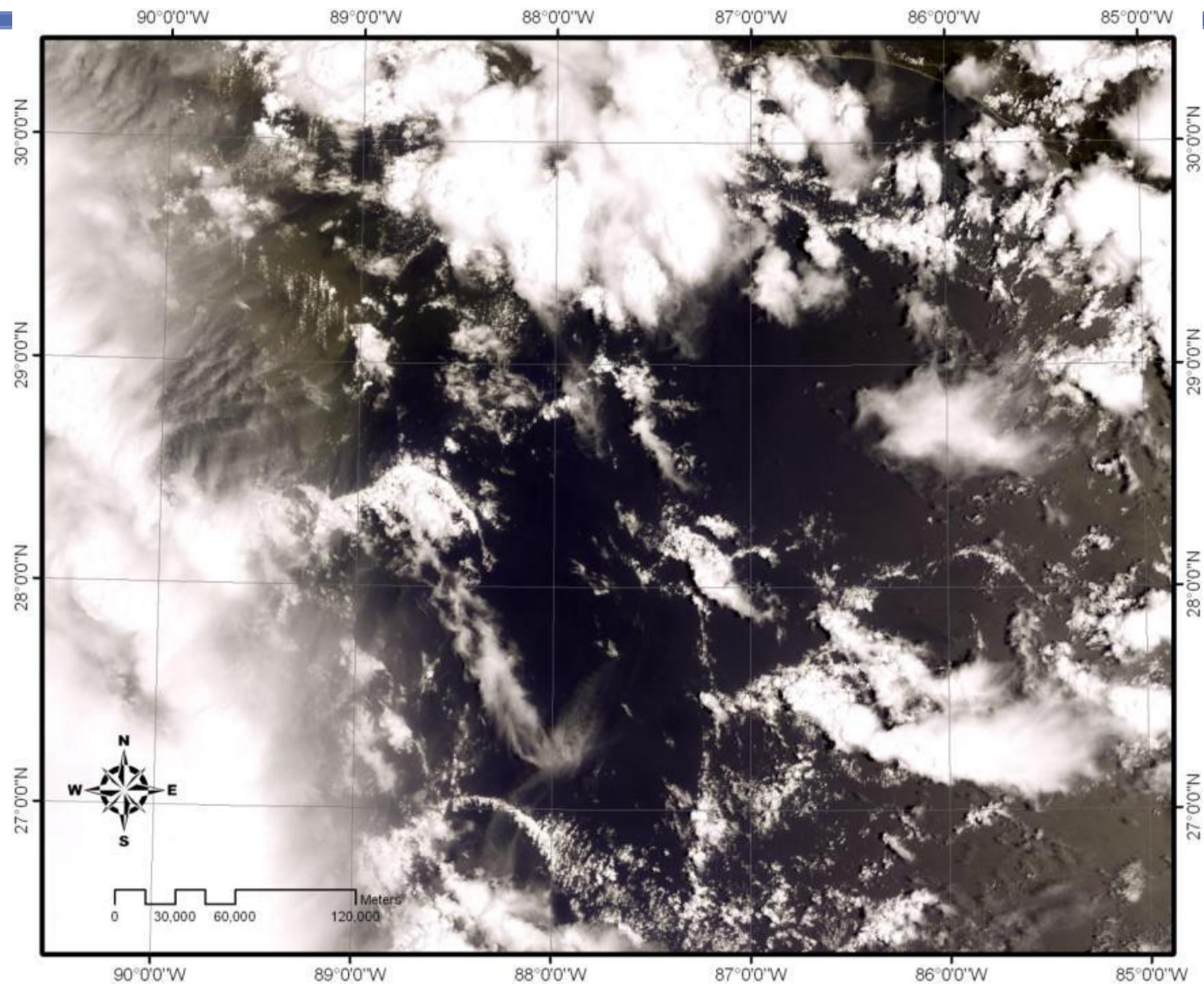
90°0'0"W
89°0'0"W
88°0'0"W
87°0'0"W
86°0'0"W
85°0'0"W
30°0'0"N
29°0'0"N
28°0'0"N
27°0'0"N
N
W
E
S
0
30,000
60,000
120,000
Meters

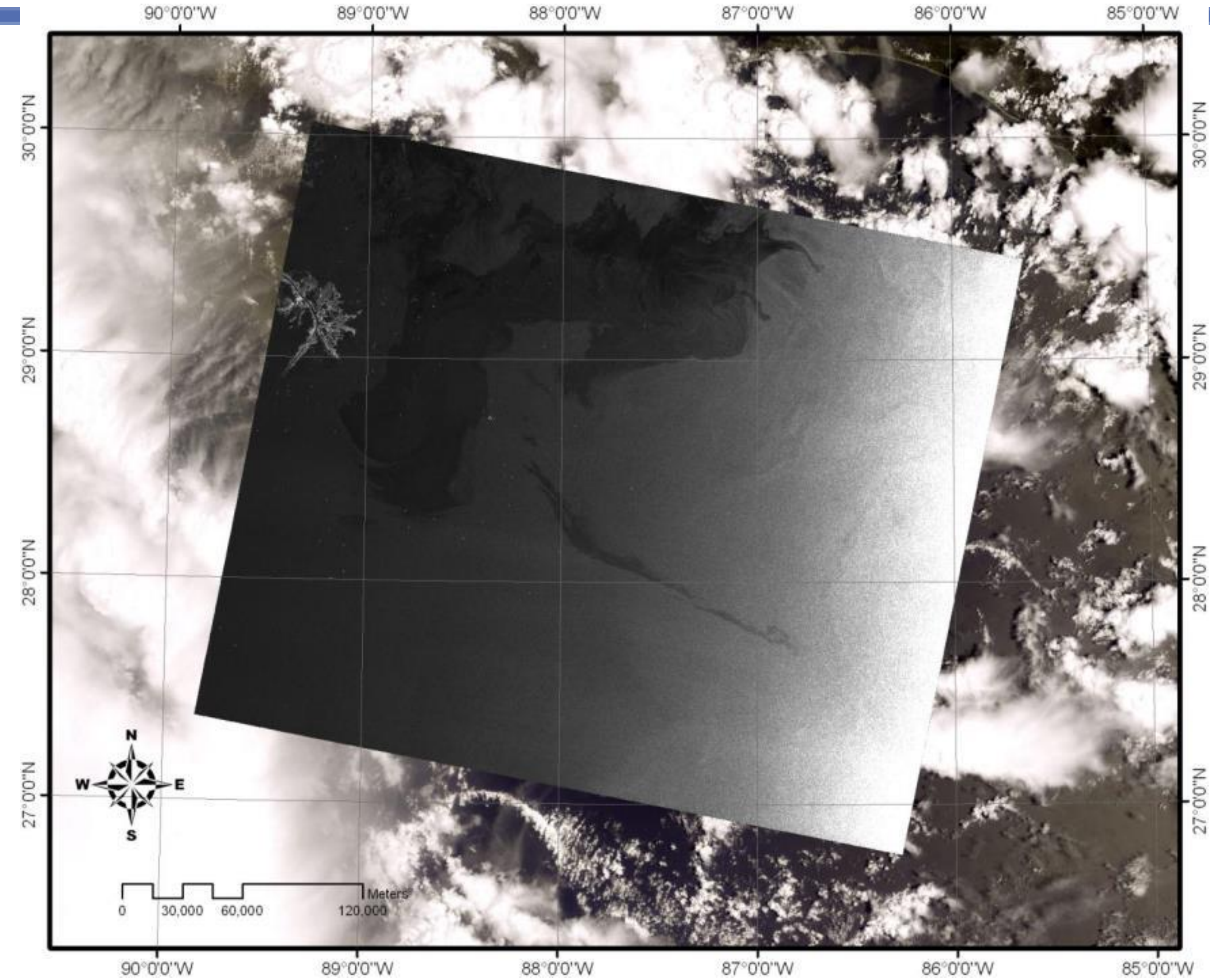

90°0'0"W
89°0'0"W
88°0'0"W
87°0'0"W
86°0'0"W
85°0'0"W
30°0'0"N
29°0'0"N
28°0'0"N
27°0'0"N
N
W
E
S
0
30,000
60,000
120,000
Meters

SAR Scenes Covering DWHD	
Envisat	123
CosmoSkyMed	140
ERS2	18
ALOS-PALSAR	70
RADARSAT 1	36
RADARSAT 2	69
TerraSar-X	30
Total	**486**

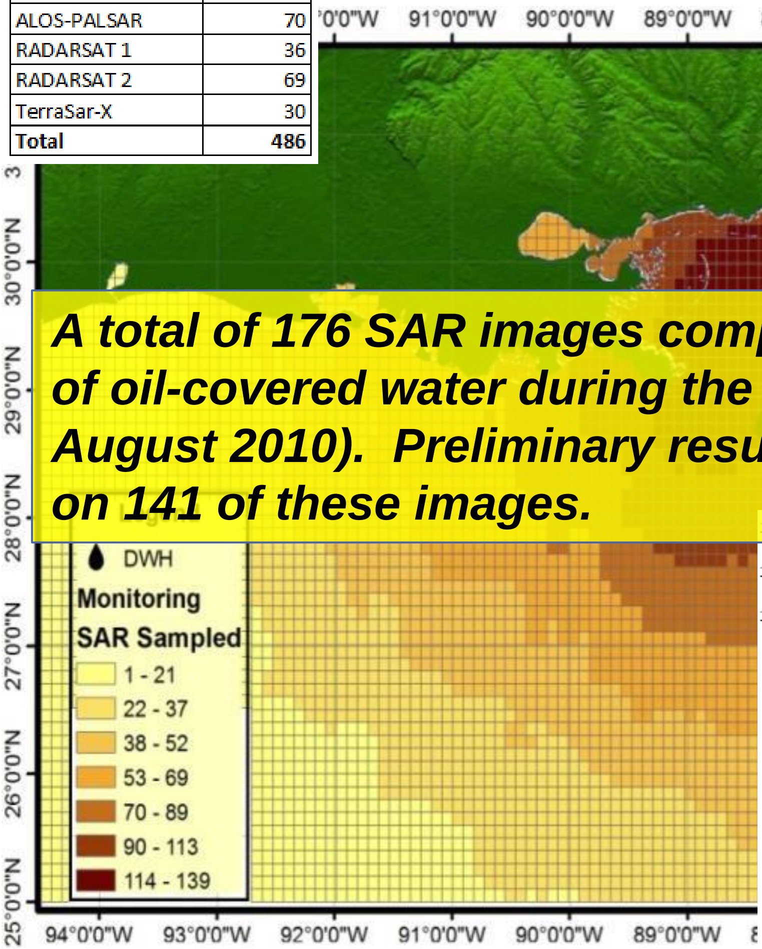

A total of 176 SAR images comprise a consistent sample of oil-covered water during the DWH episode (24 April - 08 August 2010). Preliminary results shown next are based on 141 of these images.

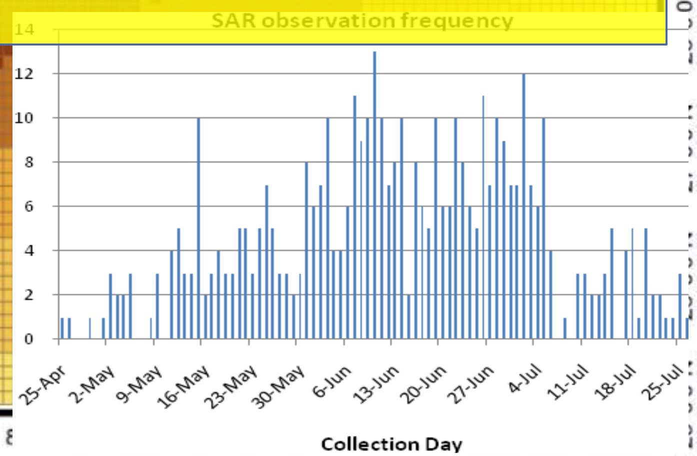

Task 2a: Oil Emulsion Detection Algorithm

- A publication for WAMOST (Garcia-Pineda, MacDonald et al. 2013) describes the development of the Oil Emulsion Detection Algorithm.
- The Deepwater Horizon spill generated large areas of rainbow sheen and smaller regions of emulsified oil.
- Comparison of aerial photos and surface samples with SAR images found that emulsion produced a radar signature with intermediate intensity between unoiled water and floating sheen.
- This signature was used to segment areas of oil emulsion in 60 SAR images, which were applied to a time-series analysis of the spill.

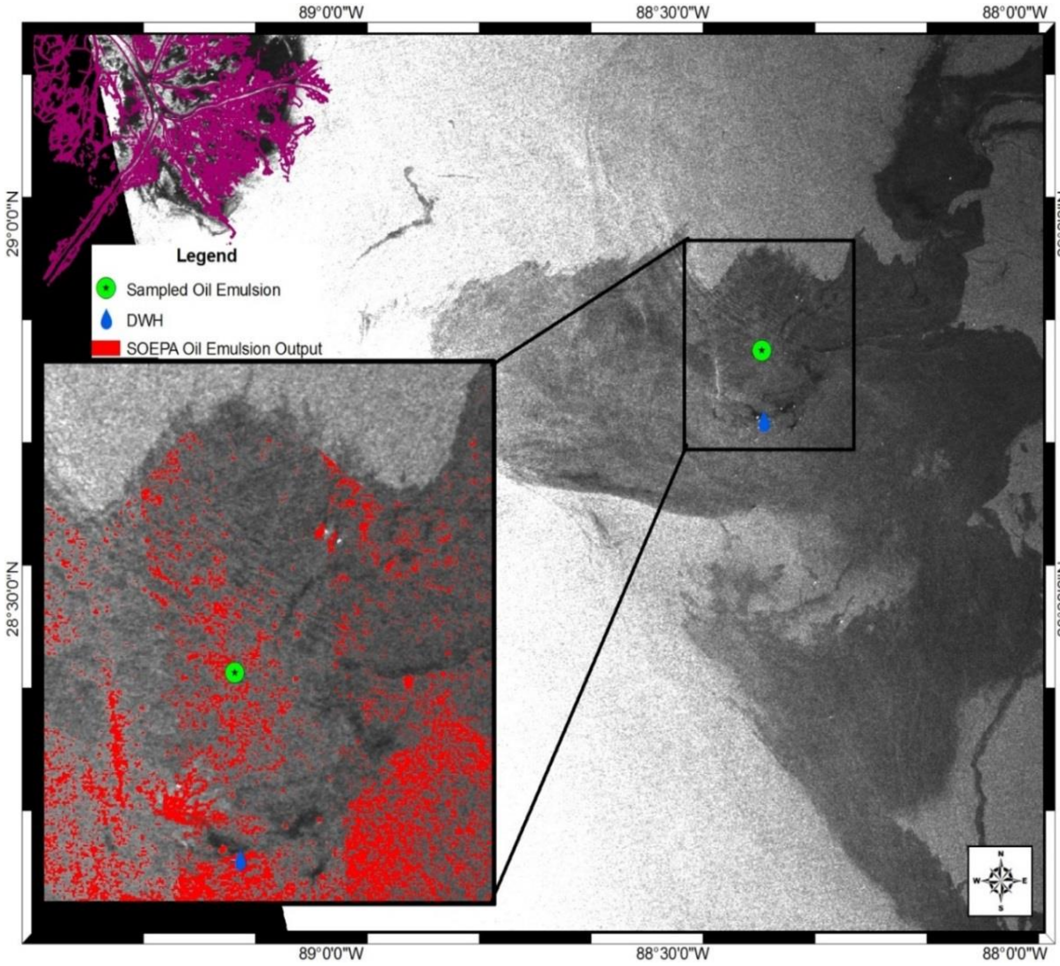

Garcia-Pineda, O. *et al.* Detection of floating oil anomalies from the deepwater horizon oil spill with synthetic aperture radar. *Oceanography* **26**, 124-137 (2013).

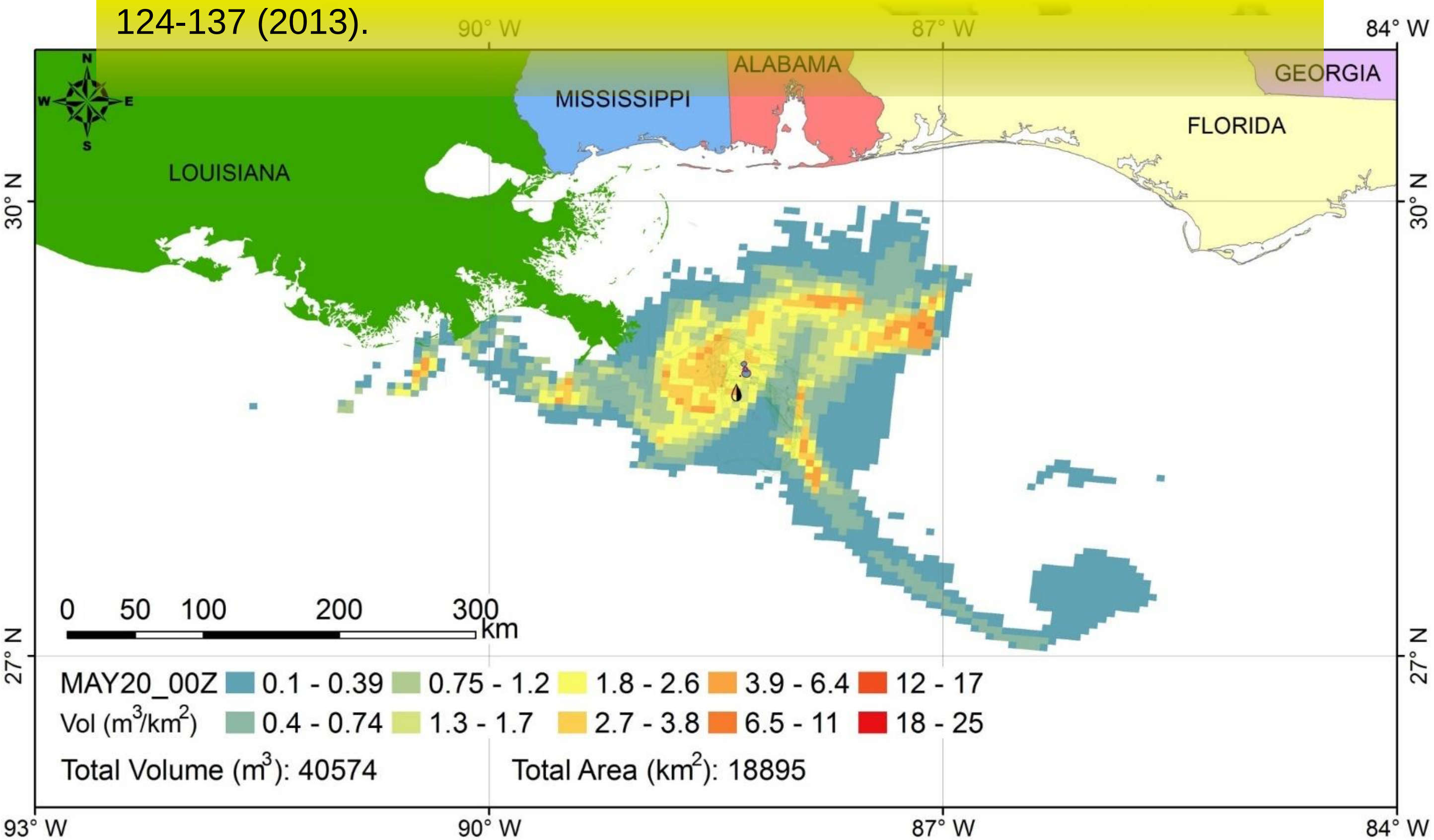

Surface volume animation: 12-h best estimate from SAR

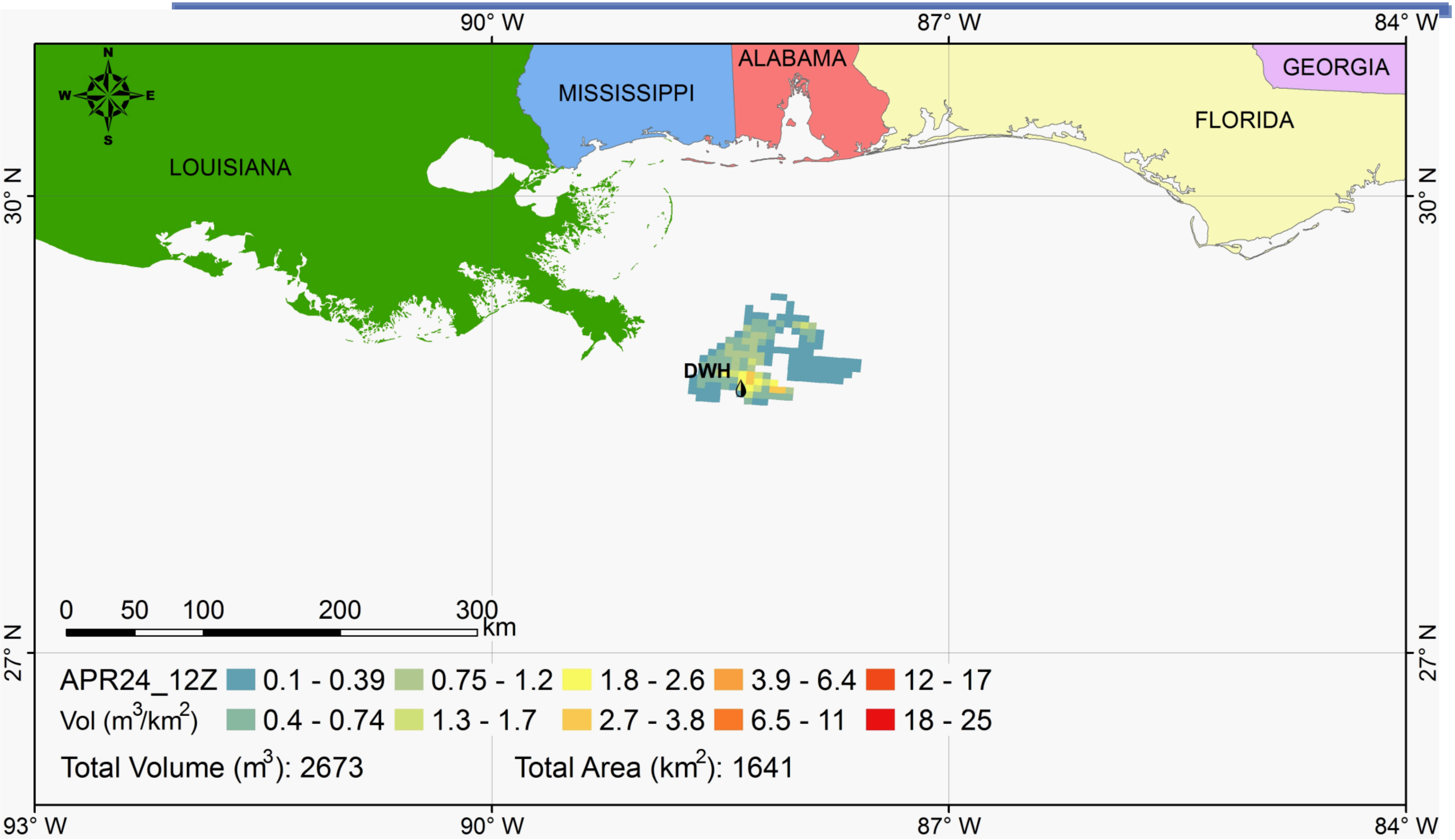

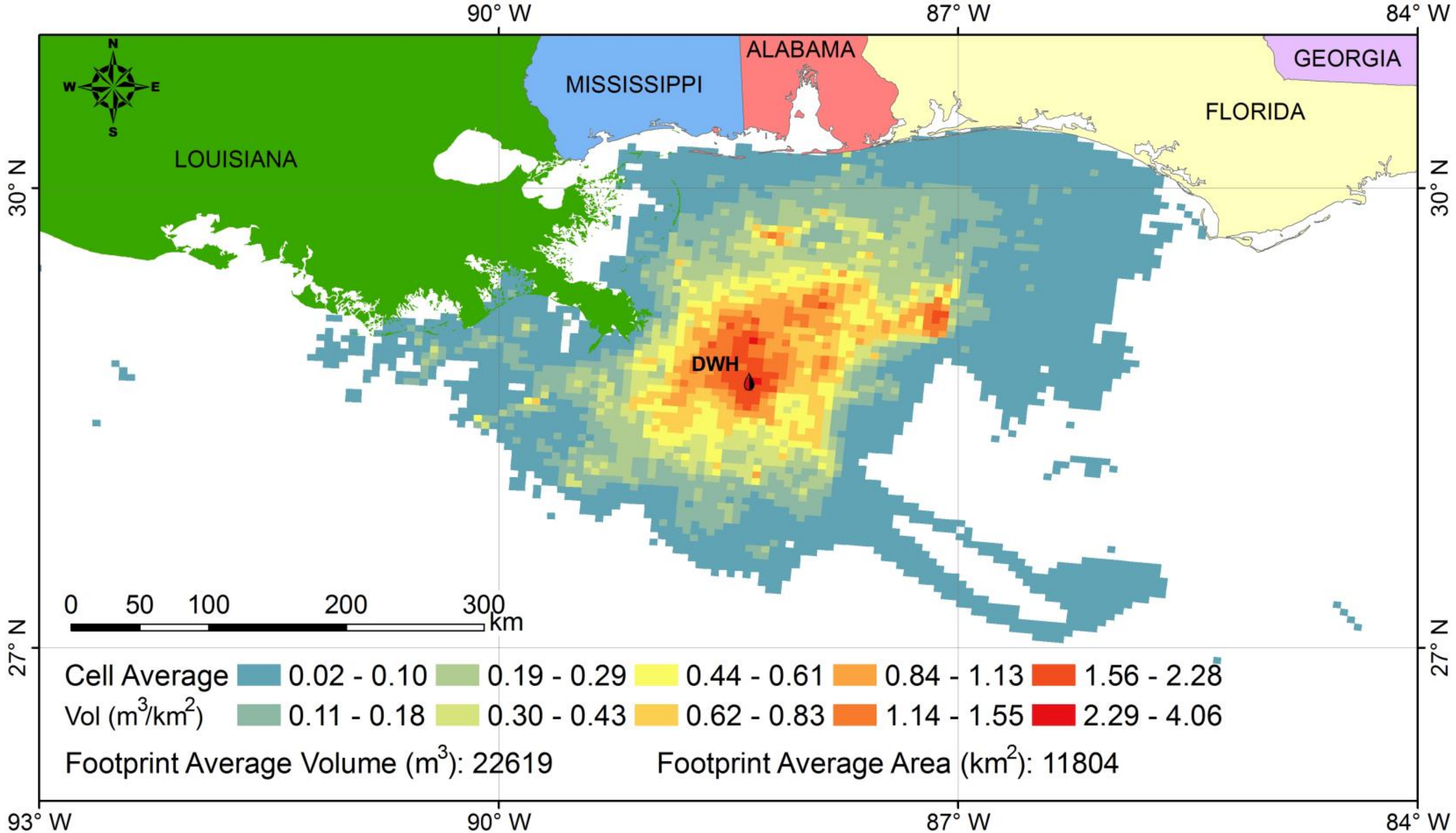

90° W
87° W
84° W
N
W
E
S
ALABAMA
GEORGIA
MISSISSIPPI
FLORIDA
LOUISIANA
30° N
DWH
0 50 100 200 300
km
27° N
Cell Average Vol (m^3/km^2)
0.02 - 0.10
0.11 - 0.18
0.19 - 0.29
0.30 - 0.43
0.44 - 0.61
0.62 - 0.83
0.84 - 1.13
1.14 - 1.55
1.56 - 2.28
2.29 - 4.06
Footprint Average Volume (m^3): 22619
Footprint Average Area (km^2): 11804
93° W
90° W
87° W
84° W

Time Series of DWH Oil
Oil-Covered Water—all thicknesses

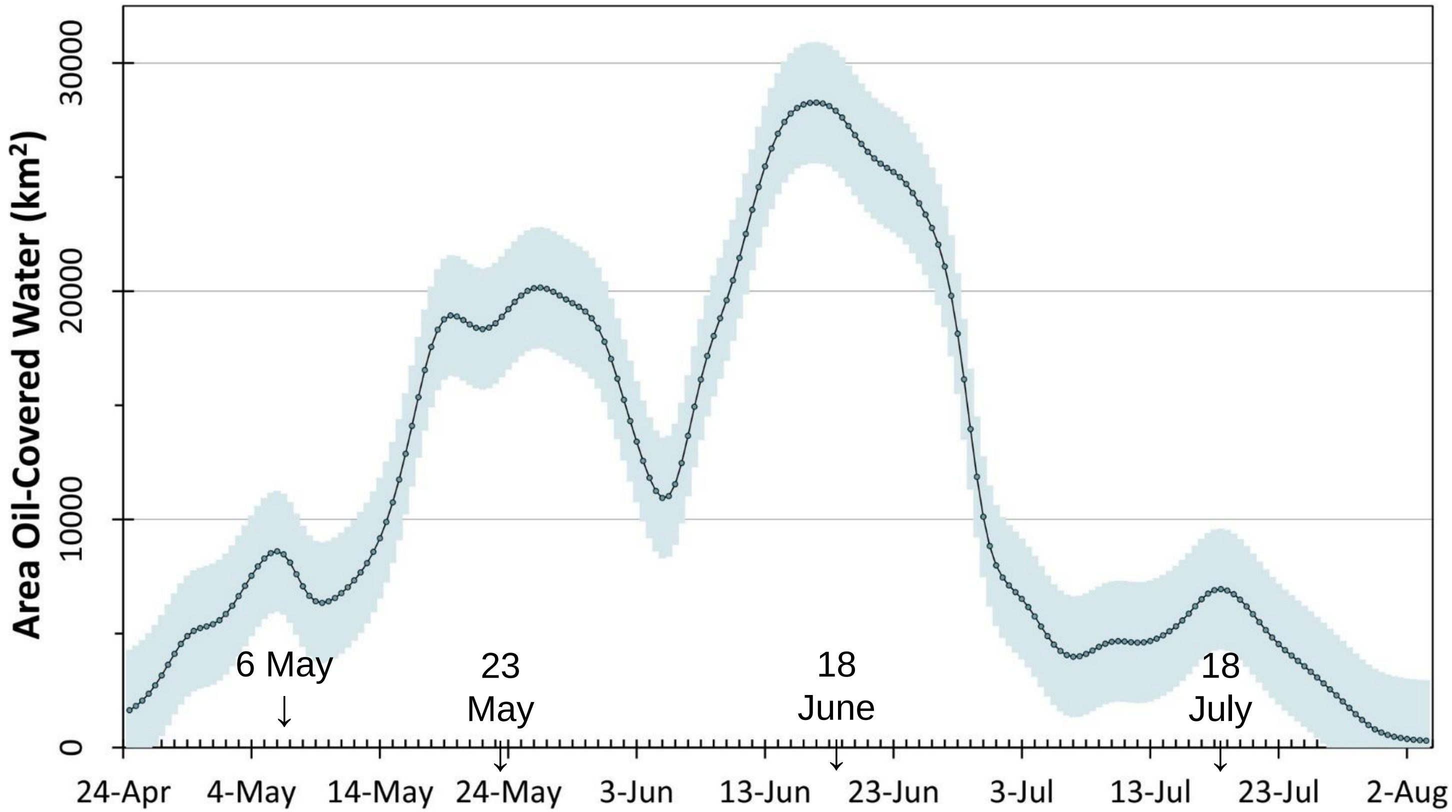

Time Series of DWH Oil
Oil-Covered Water—Thick Oil (~70 μm)

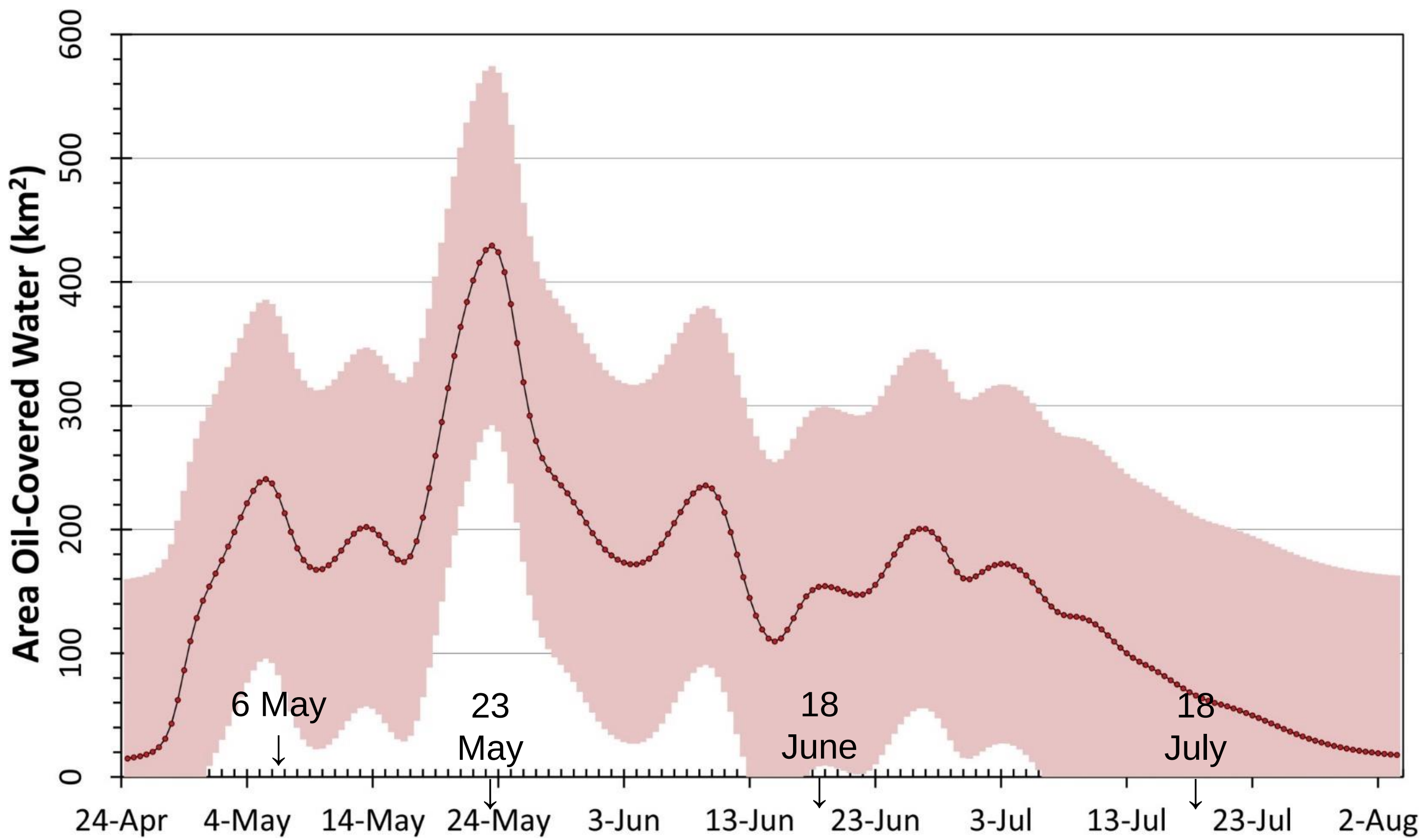

Time Series of DWH Oil
Daily SAR Volume of Surface Oil

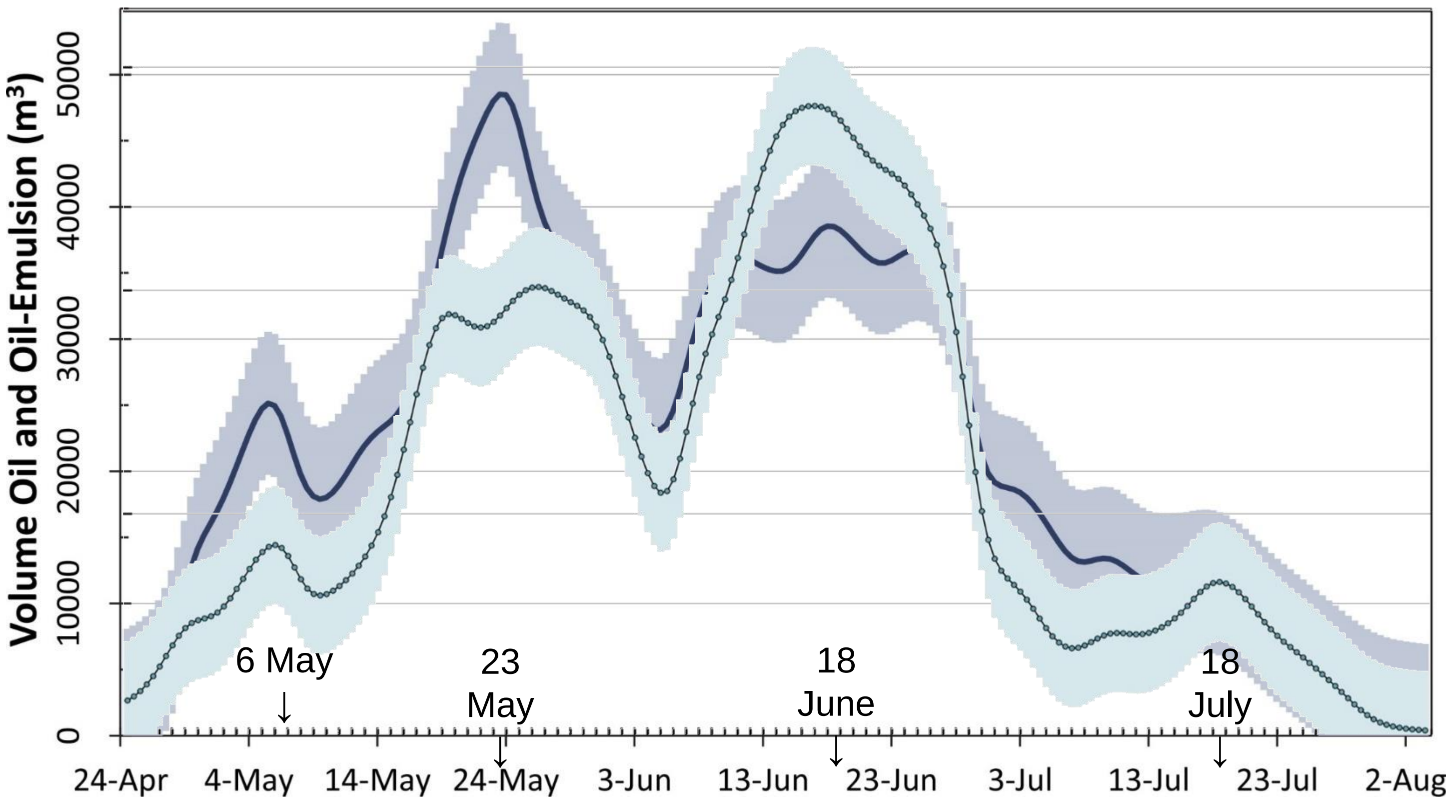

DWH Surface Oil Animation

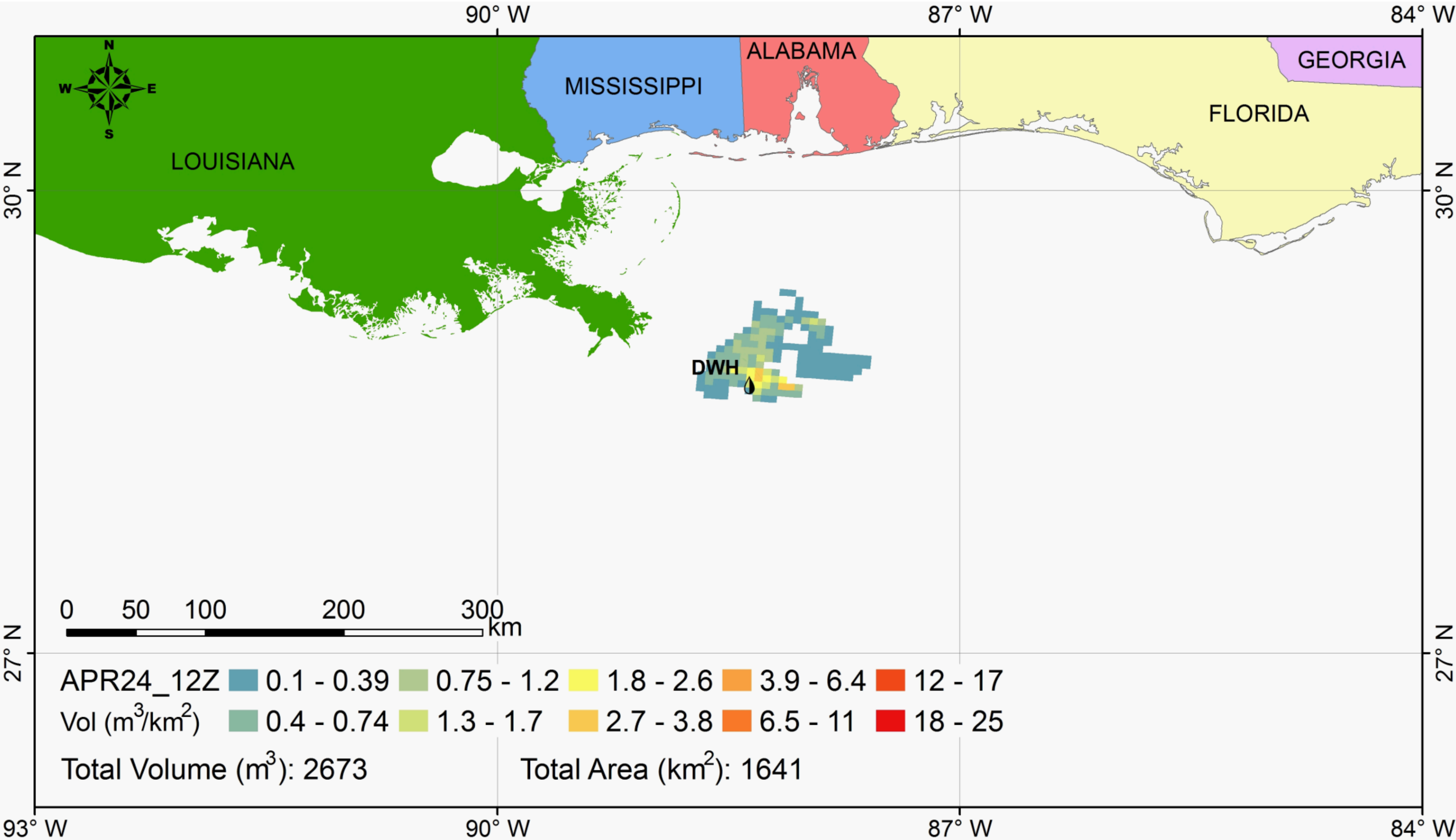

Movie S1 (1-min)

Task 2a: Characterize DwH Surface Oil Distributions Using Synthetic Aperture Radar

- Published results delineated the average distribution of DWH surface oil volume (MacDonald, Garcia Pineda et al. 2015) in units of m^3/km^2.
- A time-series of the data showed the strong effect of winds in reducing the visible volume of surface oil.
- Results indicate a reduction in volume (21%) during the June-July phase of the spill was accompanied by an increase in area (49%)

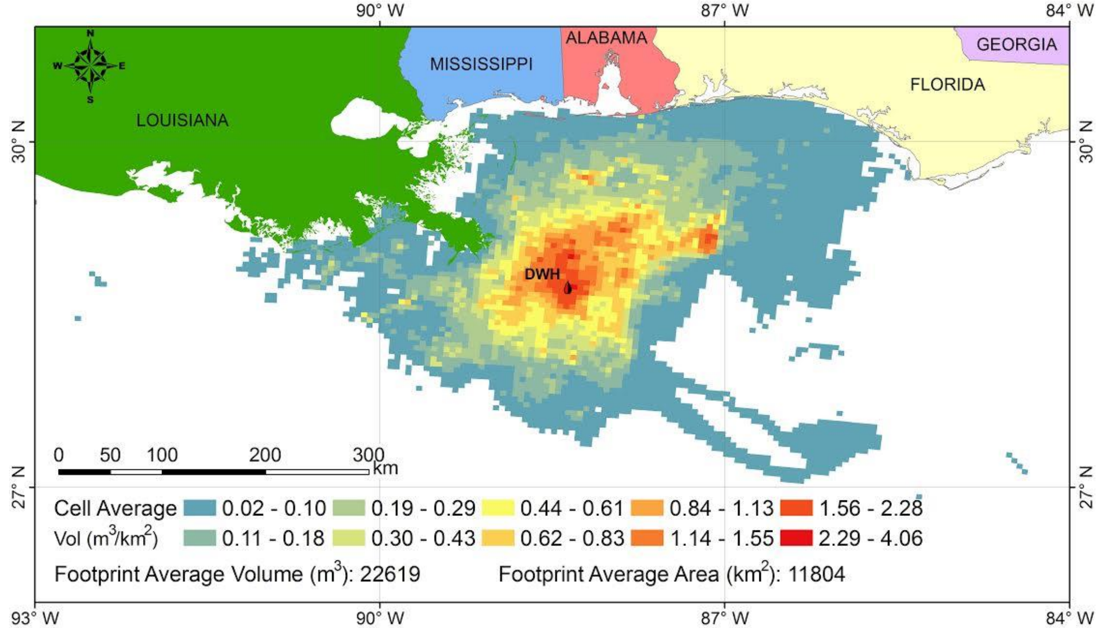

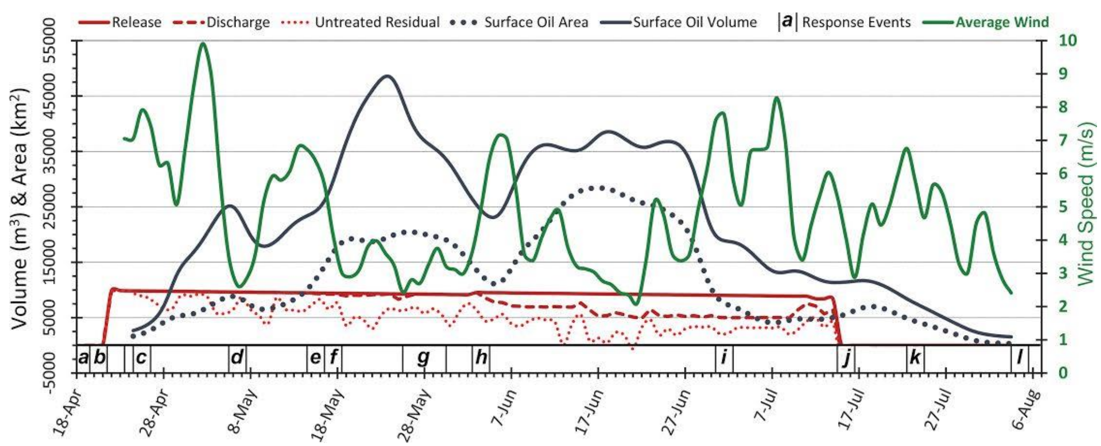

Task 3: Surface-oil Transport and Weathering Model, Forcing Fields

Objectives

- Develop a surface-oil transport and weathering model for the Gulf of Mexico.
- Compile and assess oceanographic and atmospheric forcing fields for the oil model.
- Develop validation metrics for quantifying model performance.
- Parameterize the oil transport and weathering model based on validation metrics and the remotely-sensed surface oil data.

OSCAR (Oil Spill Contingency and Response) SINTEF-Norway

Inputs

Oil type
Spill rate, location,
Special conditions
Response specifications

Coastline
Bathymetry
Currents
Waves
Wind speed
Sea temperature
Sea ice coverage
Biological resources

Processes

Drifting
Spreading
Evaporation
Photo-oxidation*
Emulsification
Natural dispersion
Dissolution
Degradation
Sediment interactions:
- Water column and seafloor
- Droplets and WAF

Stranding
Response actions:
- Chemical dispersion
- Mechanical recovery
- Burning*

Outputs

Oil mass balance,
Geographical distributions,
Properties, Biological implications

Task 3: Oil Weathering (SINTEF)

- OSCAR has previously been run with a surface or subsea release of fresh crude oil or petroleum product.
- Weathering algorithms calculate the further behavior and fate of the oil
- For the WAMOST project, OSCAR was modified to permit starting the model from a given spatial distribution of oil on the sea surface, with an estimated thickness, age and weathering history.
- This work required two innovations:
  1. Establishing a setup start-state in the software for pre-weathered oil slicks
  2. Modifying the I/O of OSCAR to output parameters required for determining weathering state of the DwH oil.
- A version of OSCAR available to the academic community has been released.

Task 3: Dispersant Effects on DwH Oil

- OSCAR model simulation of surface oil from DwH.
- Without dispersants, the volume of the spill is relatively consistent through July, when installation of the capping stack reduced the discharge rate.

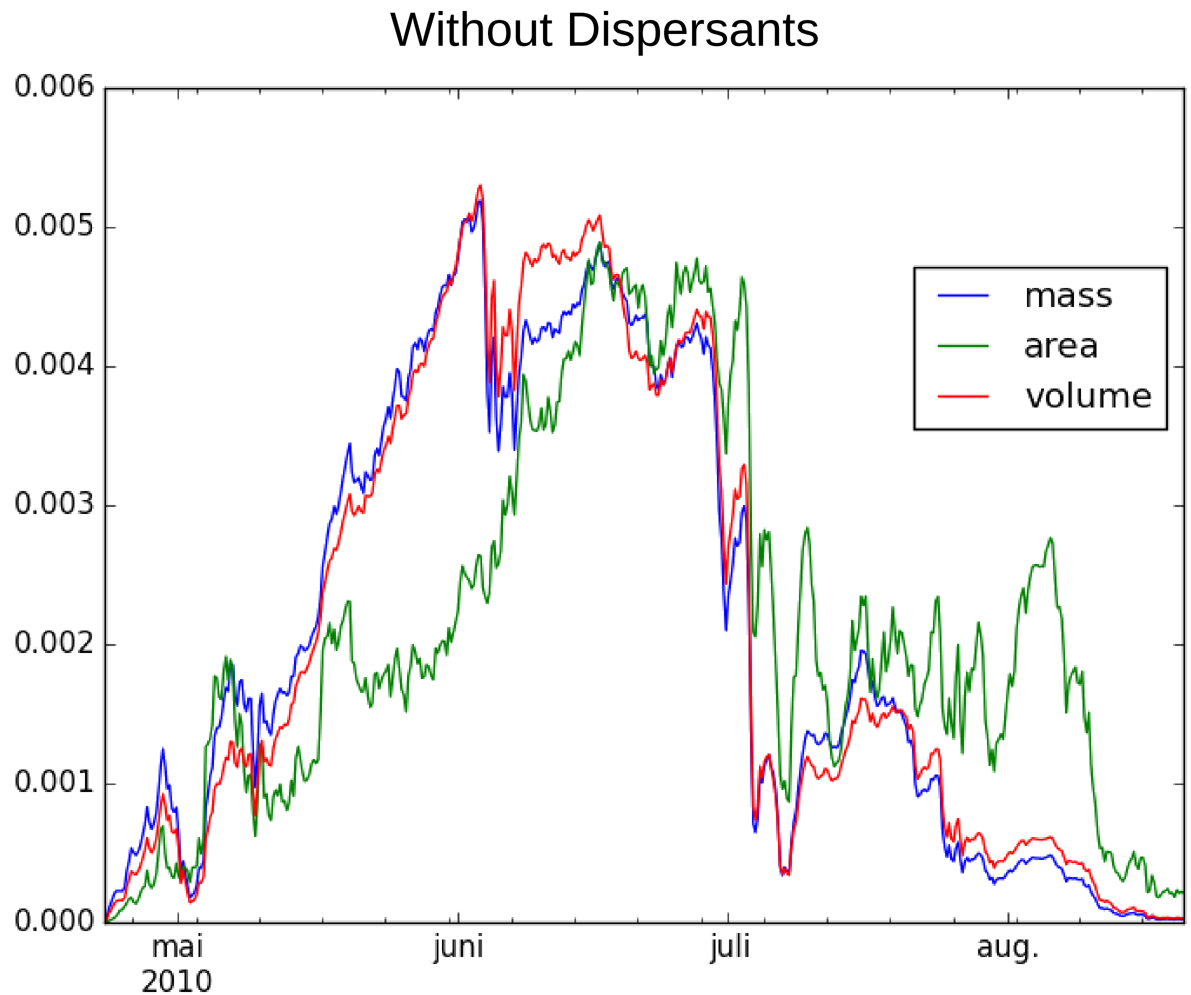

Task 3: Dispersant Effects on DwH Oil

- Modelled with dispersant application, the surface oil volume and mass decreases sharply in July.
- This coincides with increased subsurface treatment with Corexit.
- Result is consistent with WAMOST results obtained from SAR observations.

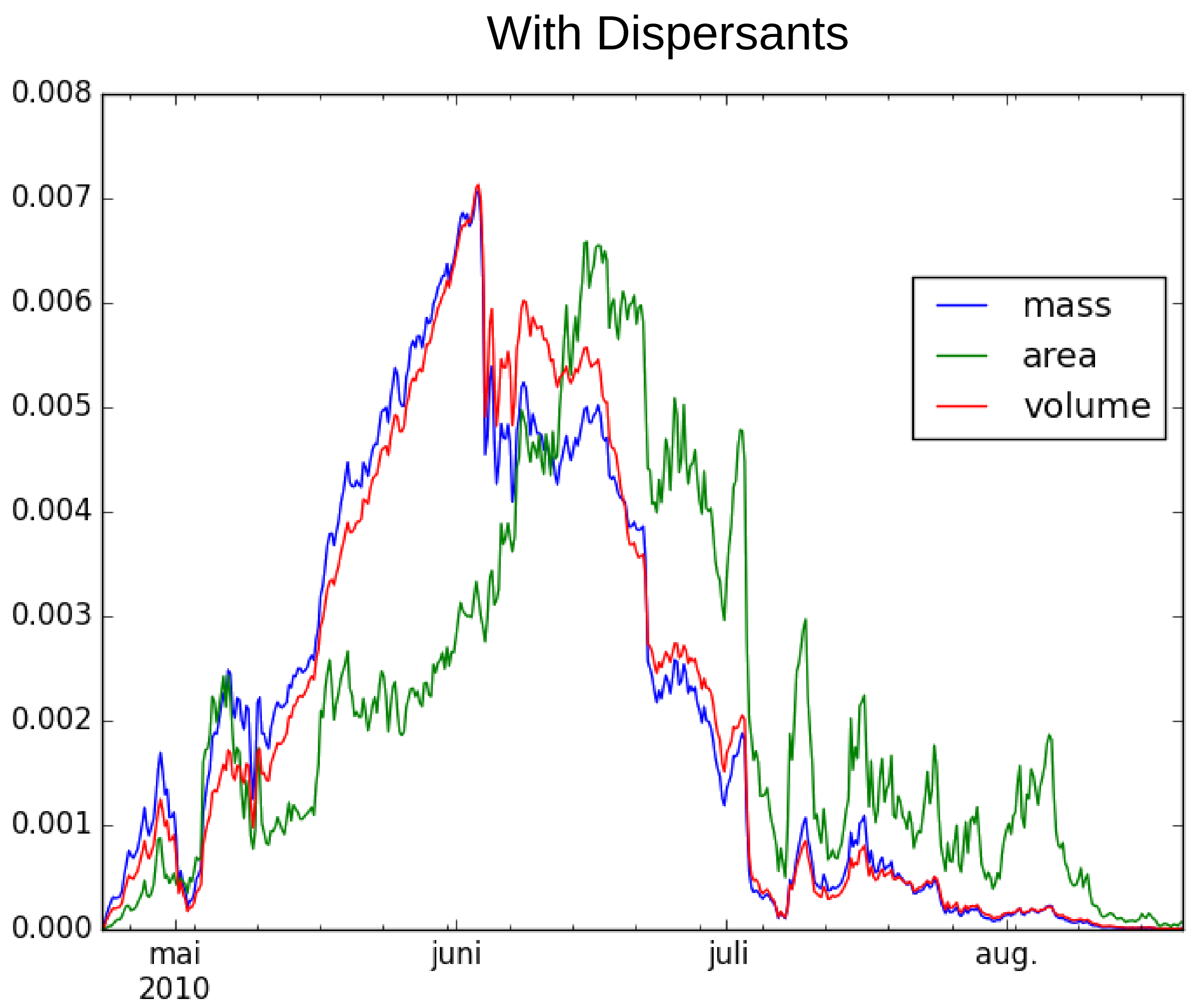


Questions
Ian MacDonald,
Florida State University

Task 3: Forcing fields, ocean currents

The Naval Oceanographic Office Operational Prediction system for the Gulf of Mexico and Caribbean (AmSeas)

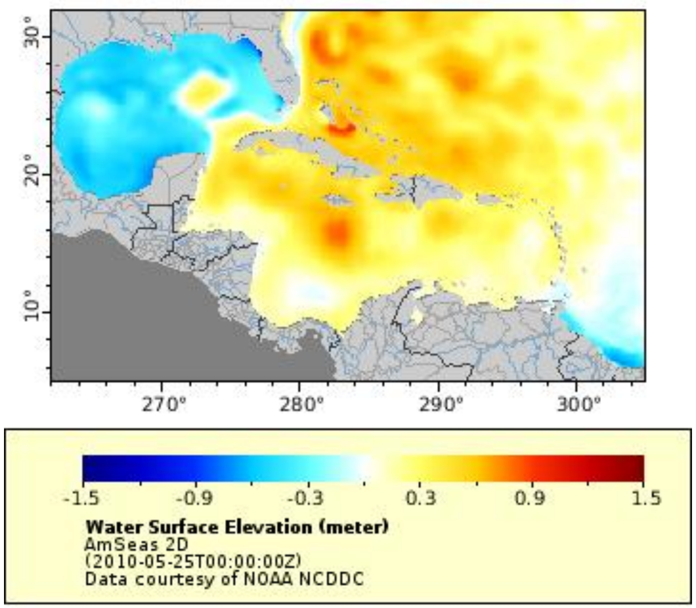

- Navy Coastal Ocean Model (NCOM), 1/36° (~3 km), 40 vertical levels (sigma-z level)
- Atmospheric forcing: Navy's COAMPS model
- Assimilation: all quality controlled observations including satellite SST and altimetry, as well as profile T and S data using NCODA system
- Data available via NOMADS: 3hr May 08 2010 – present – not the entire DwH time period.

HYCOM + NCODA Gulf of Mexico 1/25° Analysis/Reanalysis (GOMl0.04)

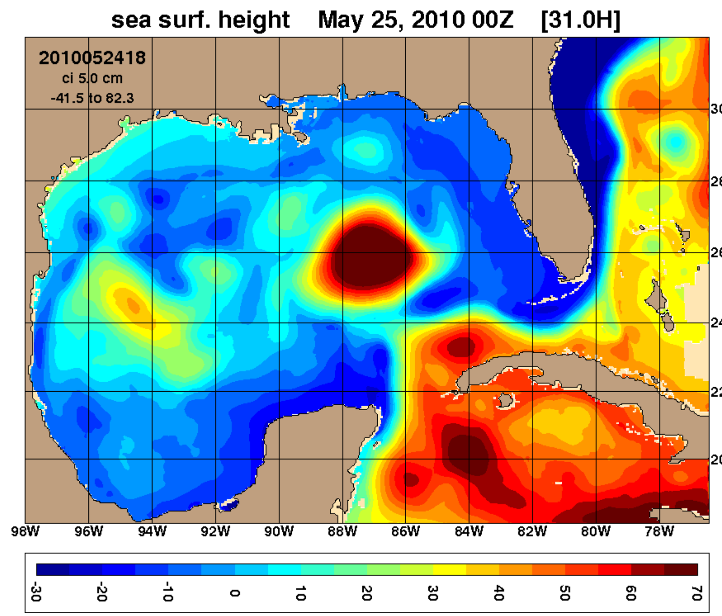

- HYbrid Coordinate Ocean Model (HYCOM), 1/25° (~4 km), 20 vertical hybrid (isopycnic/sigma/z-level) levels
- Atmospheric forcing: NOGAPS (20.1, 31.0), CFSR (50.1)
- Assimilation: all quality controlled observations including satellite SST and altimetry, as well as profile T and S data using NCODA system
- Analysis runs 31.0 (3 DVAR): Apr 2009 – 2014
  20.1 (NCODA MVOI): Jan 2001 – Jul 2010
- Reanalysis run 50.1 (3 DVAR): Jan 1993 – Dec 2012

Task 3: Near-Surface Velocity Shear in HYCOM-GOMl0.04 and NCOM-AmSeas

Vertical Grids

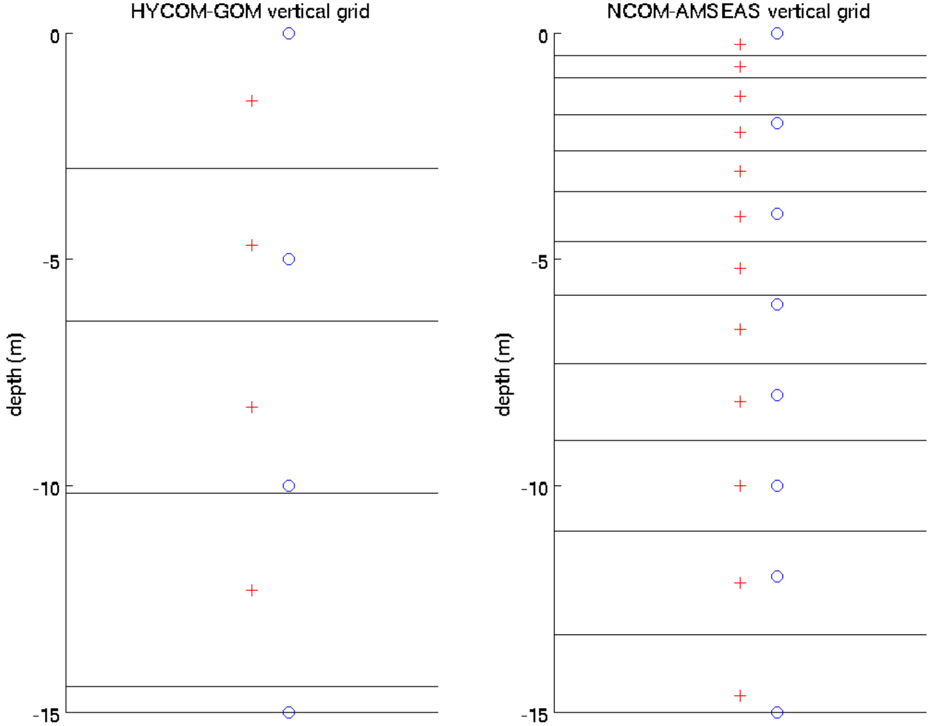

Blue circles indicate interpolated depths for model archive

Magnitude of vector difference between velocity vector of topmost grid cell and upper 10m averaged velocity

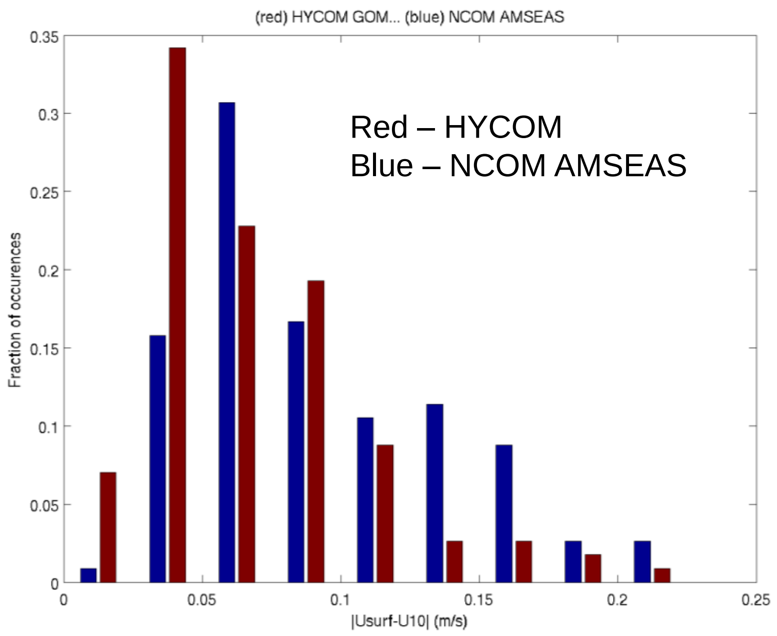

25 May – 30 Sept 2010 Daily time series near DWH

- Differences in HYCOM and NCOM shear may be due to vertical grid, wind forcing, or turbulence closure.

Task 3: Assessment of the NCOM-AmSeas and HYCOM-GOMl0.04

- Sea Surface Height (SSH):
  Models vs CCAR altimetry
  Loop Current (LC) front

- Sea Surface Temperature (SST):
  Models vs SAMOS ship data
  ARGO floats (www.nodc.noaa.gov/deepwaterhorizon/insitu.html)

- Sea Surface Salinity (SSS) and salinity profiles:
  Satellite Ocean Color Index (USF)
  ARGO floats

Task 3: Demeaned SSH fields (m) from CCAR, NCOM AmSeas and HYCOM GOMl0.04 Time-Averaged Over May 12 – 19 of 2010

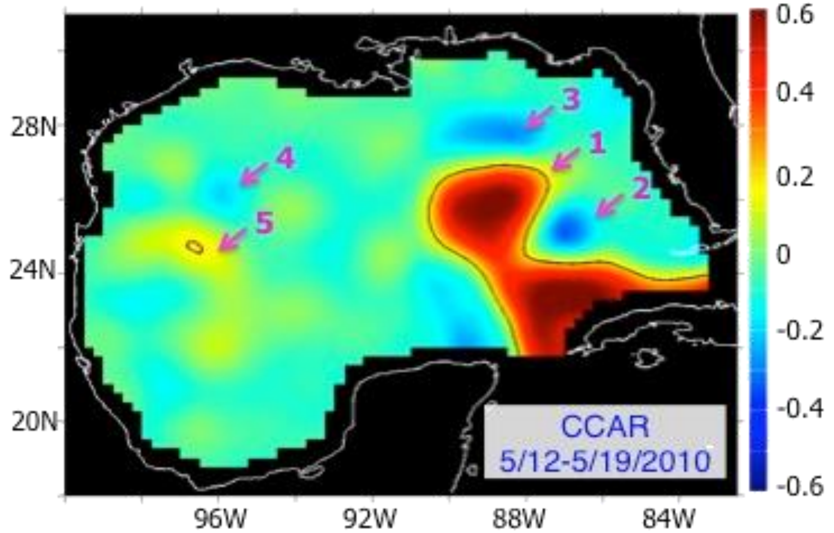

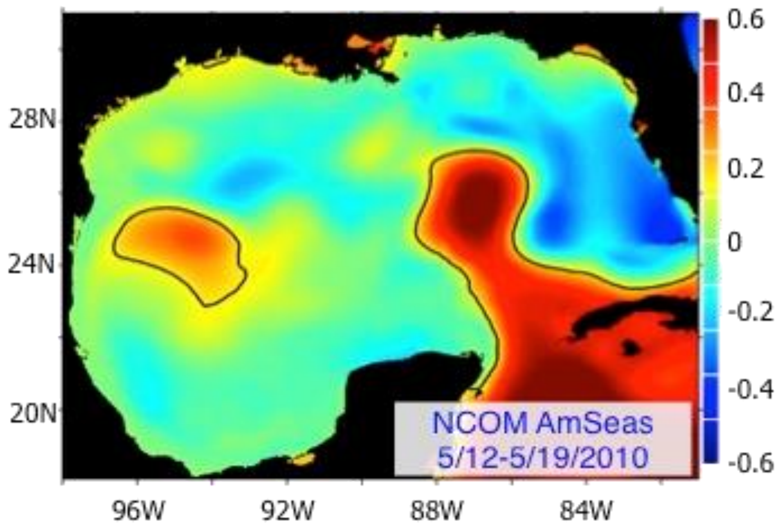

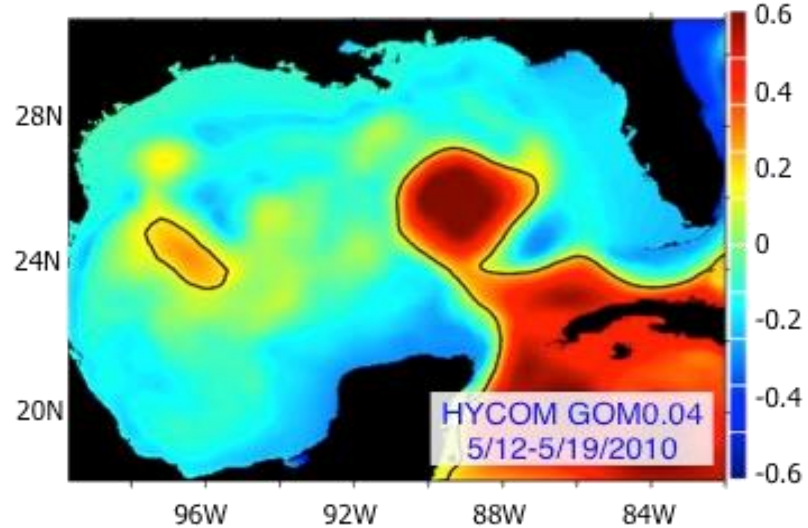

USF UNIVERSITY OF SOUTH FLORIDA

SINTEF

Task 3: LC and LCE Fronts in NCOM and HYCOM

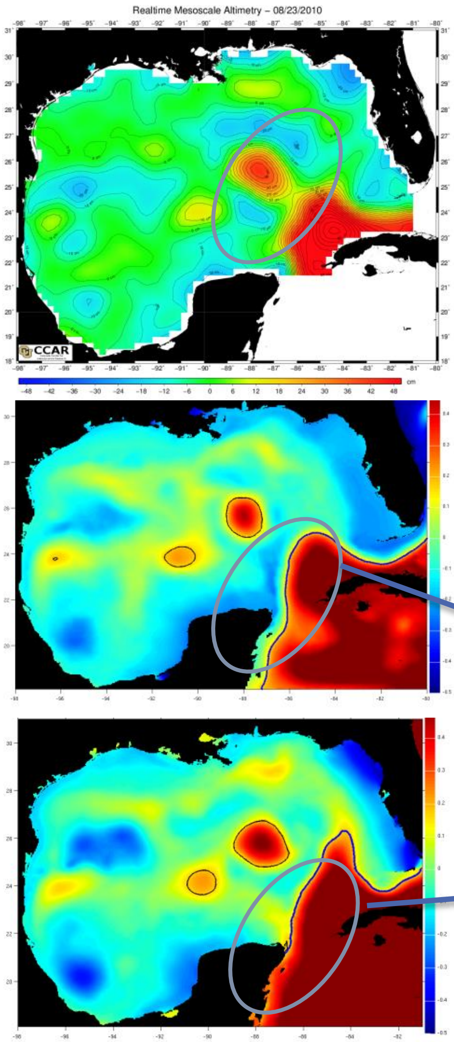

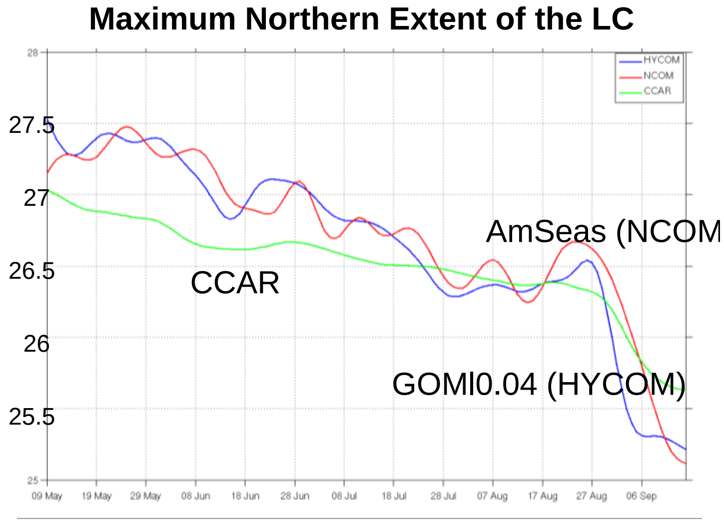

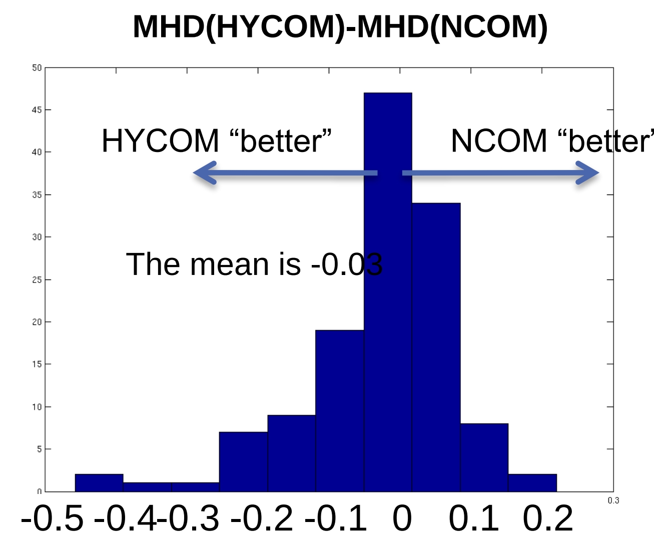

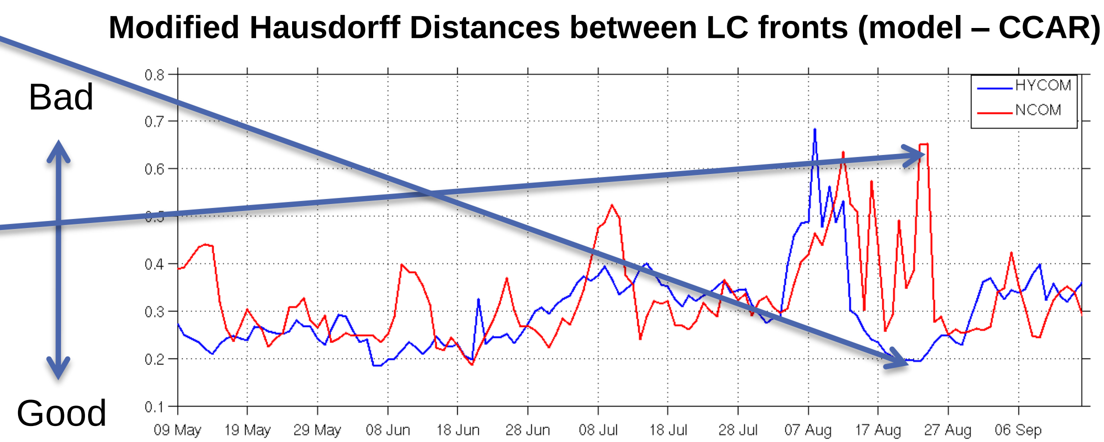

UNIVERSITY OF SOUTH FLORIDA

Task 3: Representation of the Near-surface Ocean Circulation in HYCOM GOMl0.04 Analysis (20.1 and 31.0) and Reanalysis (50.1) Datasets

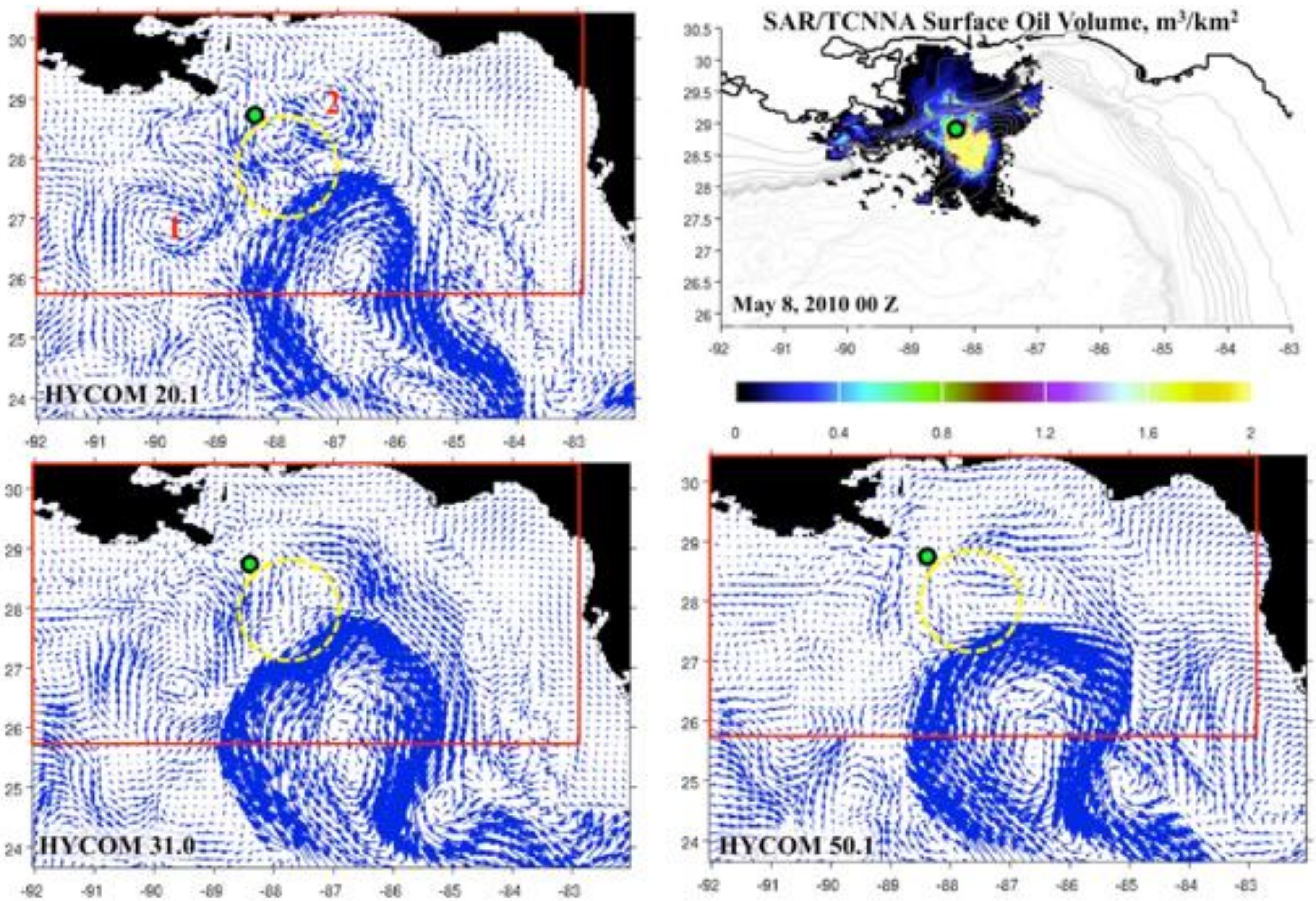

Task 3: Sea Surface Salinity in the Models vs Ship Observations During the DwH Oil Spill Event

SSS & Ship Tracks, April-August 2010

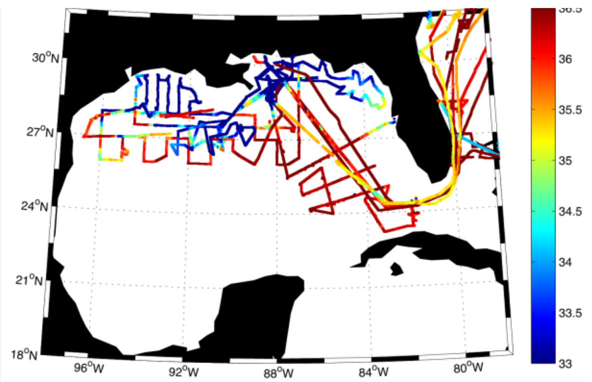

- SST and SSS fields from the analysis data sets are compared to the ship observations collected in the area during the DwH spill event
- The data were provided by the Shipboard Automated Meteorological and Oceanographic System (SAMOS)

NCOM

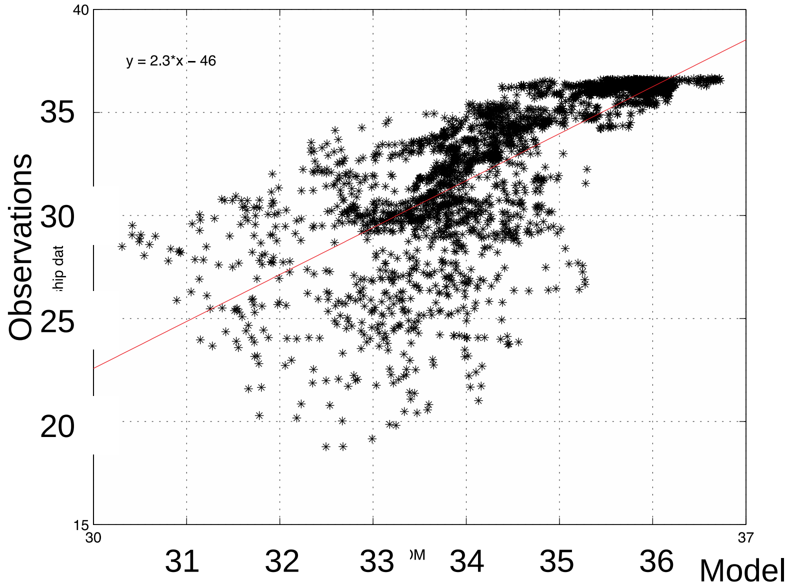

HYCOM

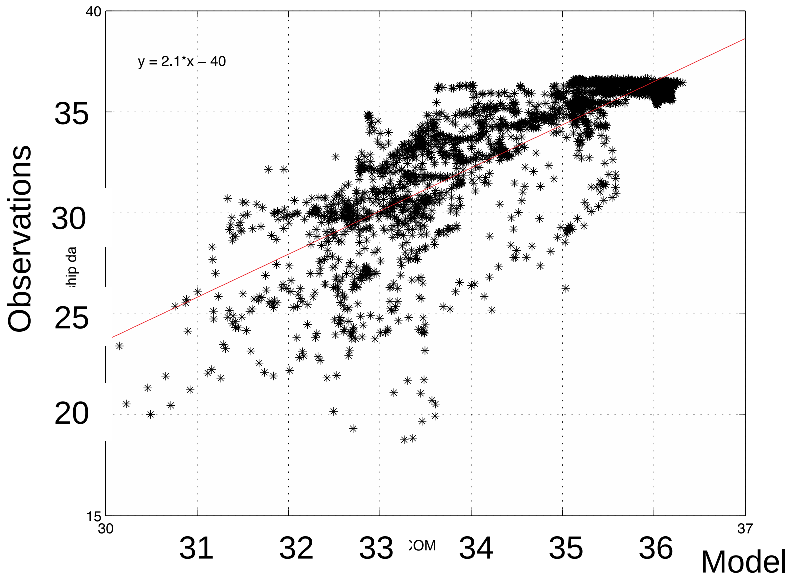

FLORIDA STATE UNIVERSITY 1851

COAPS

USF UNIVERSITY OF SOUTH FLORIDA

SINTEF

Task 3: SST in the Models vs Ship Observations

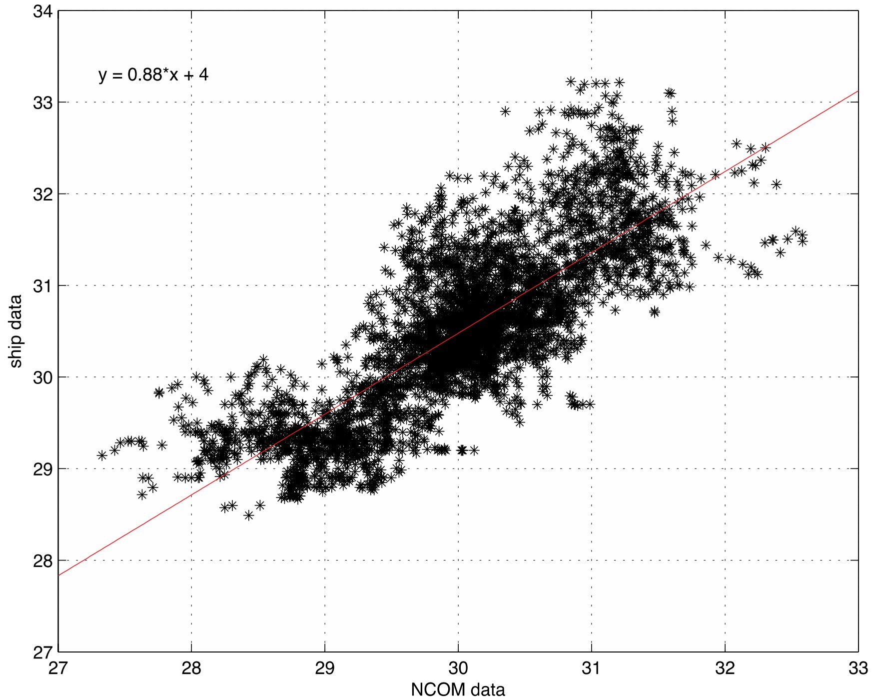

NCOM

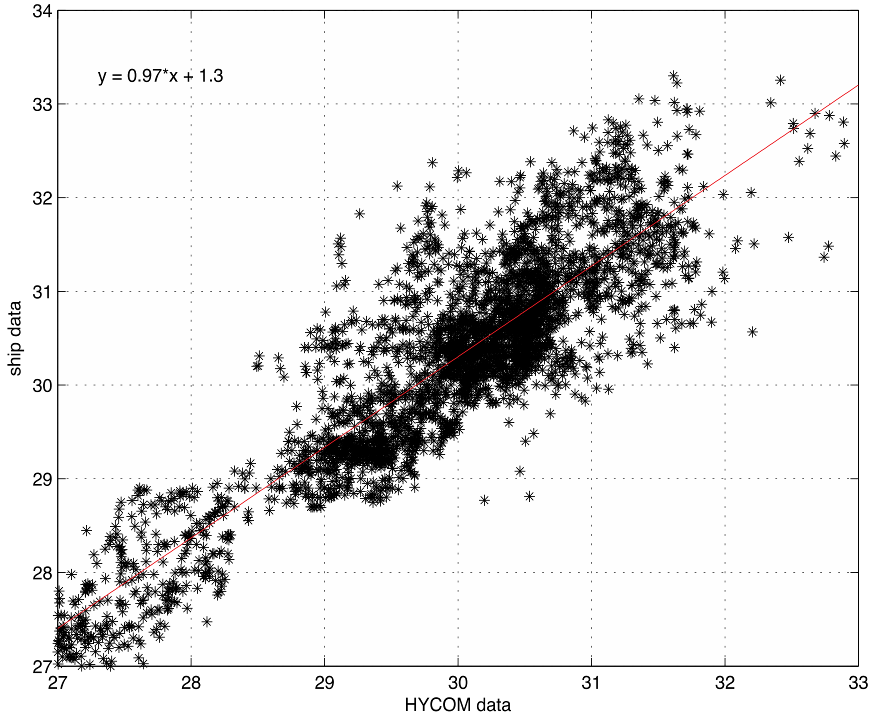

HYCOM

Task 3: T/S Profiles from the Models vs ARGO Floats

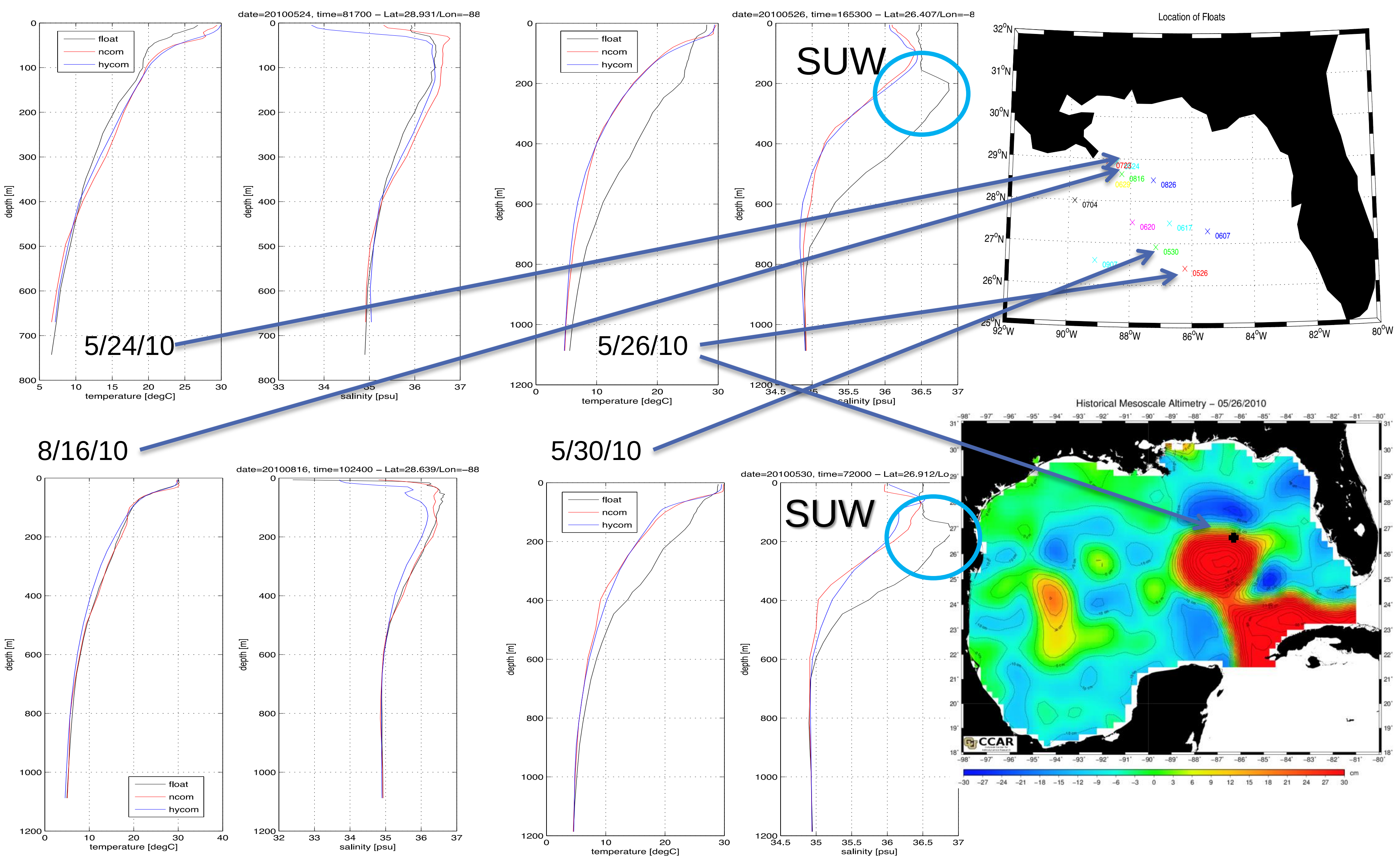

Task 3: SSS Fronts in NCOM-AmSeas and HYCOM-GOML0.04

Top: SSS from NCOM-AmSeas 7-day composite: August 1, 2010
Bottom: SSS from HYCOM-GOMl0.04 7-day composite: August 1, 2010

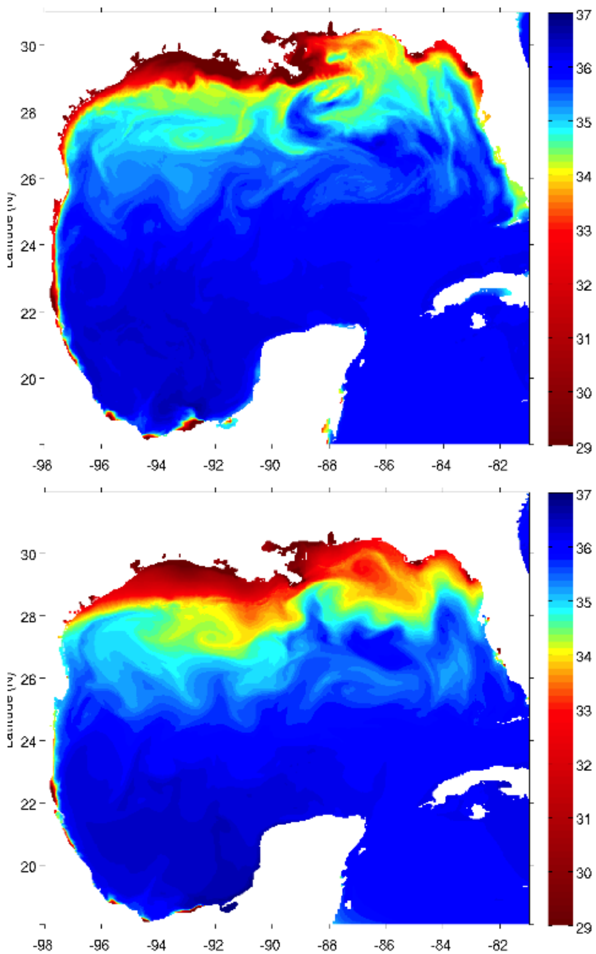

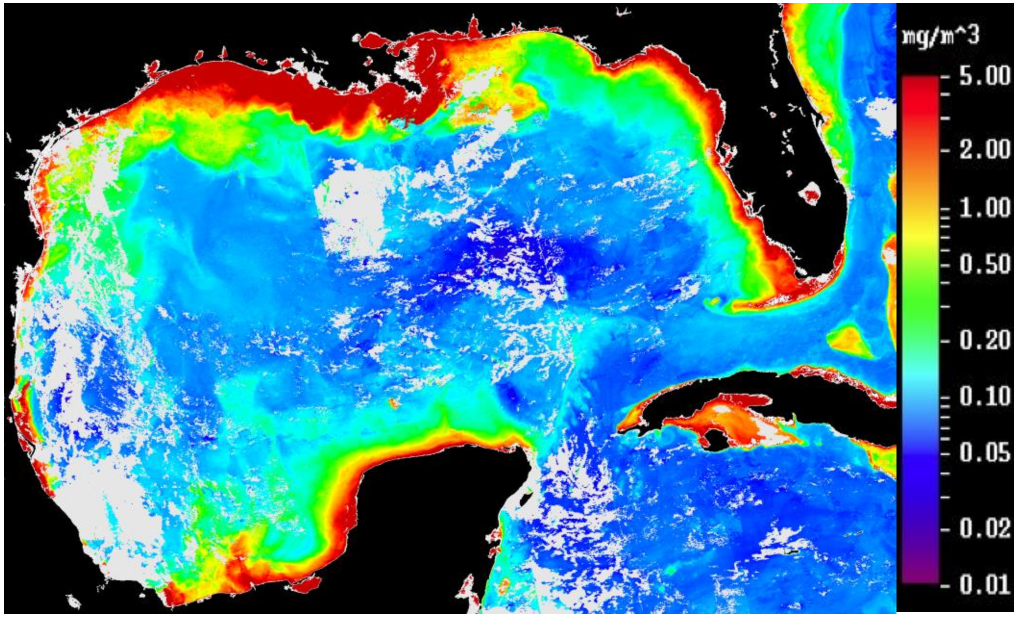

Ocean Color Index 7-day composite: August 1, 2010

Task 3: Comparison of Simulated River Plumes Using Chl-a (ocean color index)

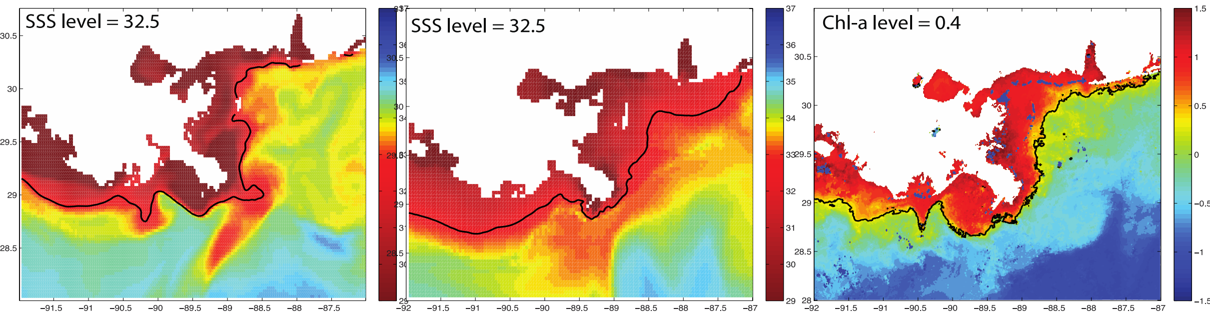

Spatial correlation between model SSS and Chl-a

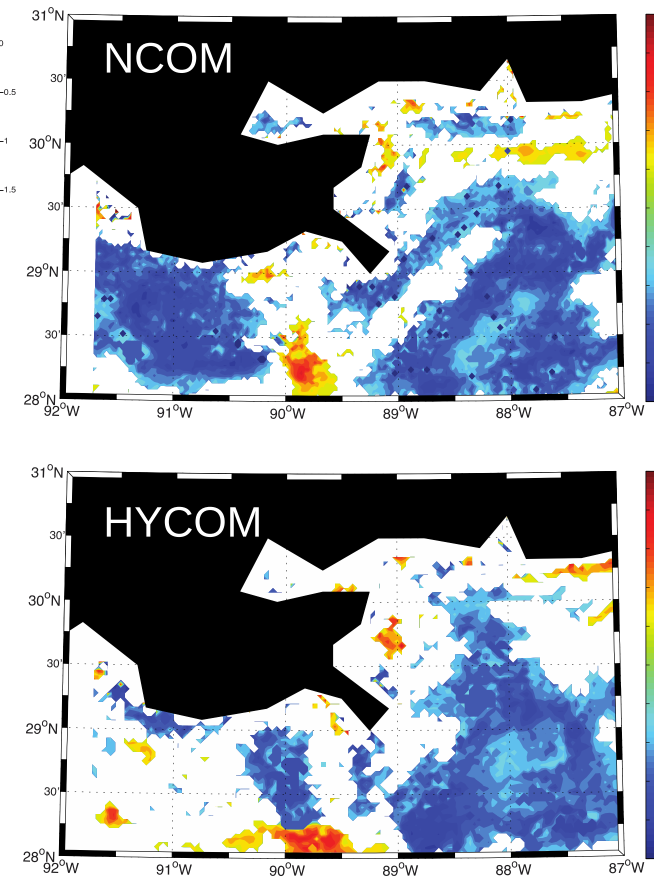

Mean MHD for OCI – HYCOM and OCI-NCOM

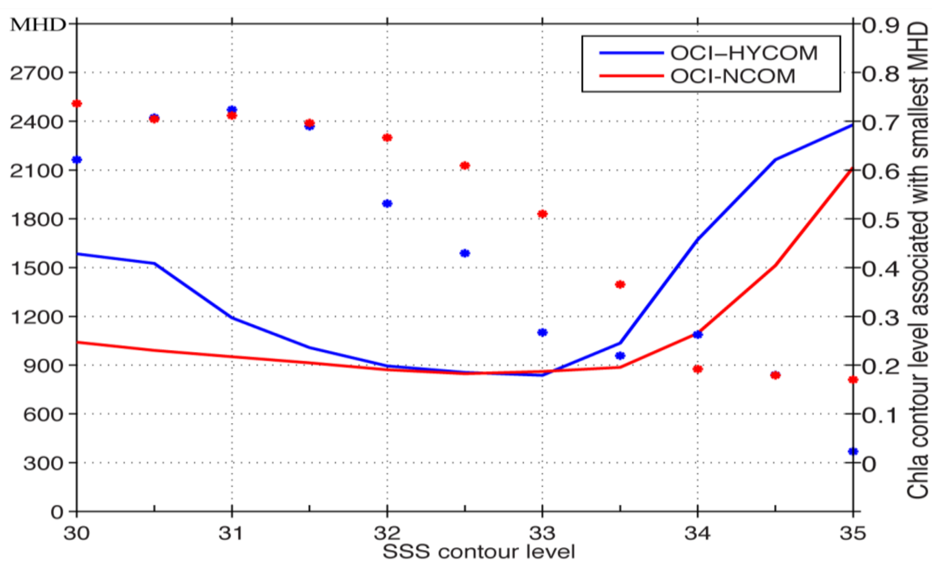

Task 3: Summary: NCOM-AmSeas vs HYCOM-GOMl0.04

- SSH:
  - ✓ Both models represent timing, location and shape of anticyclonic eddies and the Loop Current fairly well compared to CCAR data
  - ✓ There is less agreement between the model and altimeter data on position and shape of cyclonic eddies and smaller scale features
  - ✓ Fronts of the LC and LC eddies are accurately simulated in both models. On average, HYCOM has a slightly better representation of the fronts compared to NCOM.
- SSS and vertical profiles:
  - ✓ From OCI analysis, NCOM has a better representation of the river plume near the coast compared to HYCOM. Specifically, HYCOM has a more dispersed river plume and its low salinity water spreads farther offshore than in the NCOM forecast.
  - ✓ Overall, the vertical T and S profiles in both model analyses match the ARGO floats (except for the cases when ARGO float was close to a mesoscale feature).
- SST:
  - ✓ Both models demonstrate good agreement with ship observations. HYCOM has a slightly better correlation with ship data.
- Velocity fields:
  - ✓ In the deep ocean: strongly influenced by mesoscale eddies
  - ✓ In the shallow regions: winds control ocean circulation
  - ✓ HYCOM has a stronger vertical shear in the upper layers

Task 4: Wind Forcing

- For oil simulation, the near-surface ocean currents should be dynamically consistent with the wind field to avoid possible discrepancies between the wind fields and surface currents (largely influenced by winds) forcing the oil simulation
- In case when ocean surface currents are from a numerical simulation, such consistency is provided when atmospheric fields forcing the ocean model are used to derive the near-surface winds.

Considered wind fields for oil simulations:

Wind Data	Temporal Resolution	Spatial Resolution	Spatial Coverage	
Coupled Ocean-Atmosphere Mesoscale Prediction System (COAMPS)	3 hr	0.2°	120°W–60°W, 0°N–32°N	Needs validation
NCEP Climate Forecast System Reanalysis (CFSR)	1 hr	0.25°	Global	Validated in Wallcraft et al., 2009; Sharp et al., 2015
Navy Operational Global Atmospheric Prediction System (NOGAPS)	3 hr	0.5°	Global	Validated in Wallcraft et al., 2009
Cross-Calibrated Multi-Platform Ocean Surface Wind Vectors (CCMP)	6 hr	0.25°	0°W–360°W, 78.7°S–78.7°N	Validated in Atlas et al., 2009

Analysis:

- The RMS difference
- Wind speed bias
- Wind vector difference
- Timing and structure of fronts
- Comparison to NDBC observations

Task 4: Frontal Structure in CCMP and COAMPS

May 3, 2010 12UTC

Surface Weather Map

http://www.hpc.ncep.noaa.gov/dailywxmap/index_20100503.html

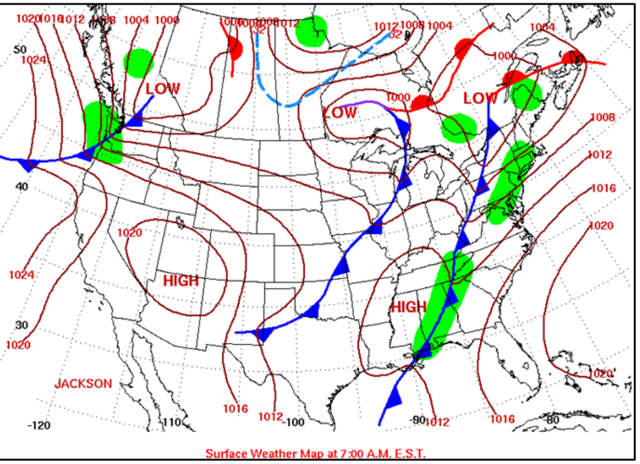

CCMP Wind Vectors

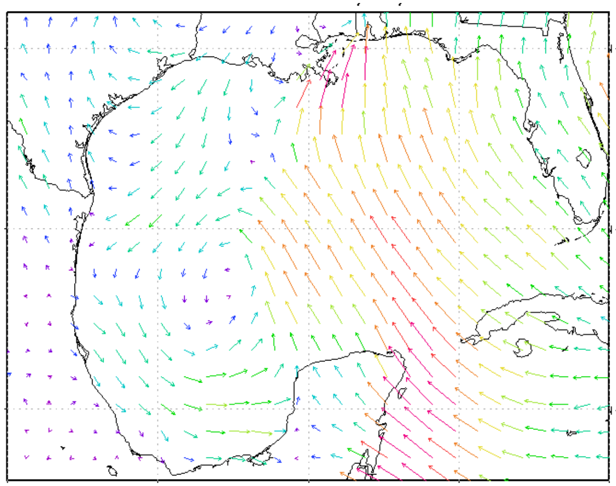

COAMPS Wind Vectors

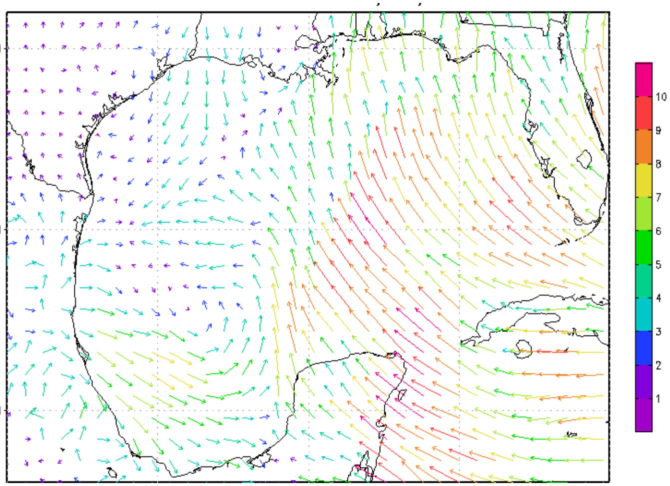

- The frontal structure is similar between CCMP and COAMPS.
- COAMPS has much larger wind speeds ahead of the front.
- In contrast, CCMP has stronger winds behind the front.
- Interestingly, CCMP also has a wind speed maximum located over the oil slick area that is not seen in the COAMPS wind vector plot.

Task 4: Wind Forcing: COAMPS vs CCMP winds

Average Wind Speed Bias and Wind Vector Difference (CCMP-COAMPS)

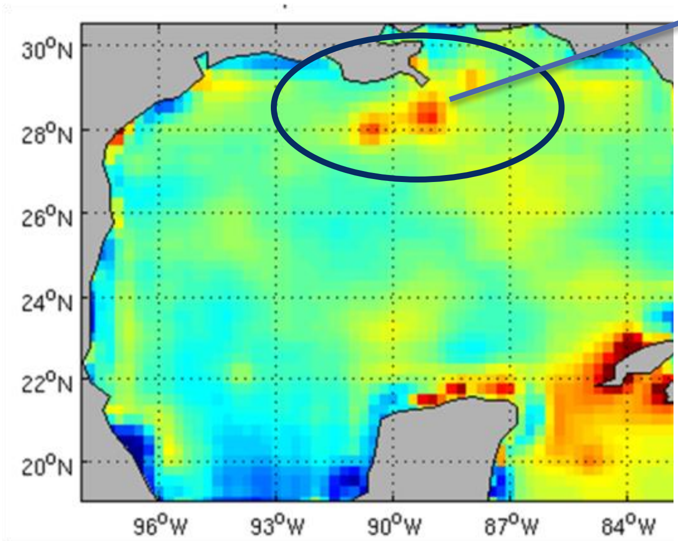

NDBC buoy 42040 surface winds and SSM/I wind speed retrieval after the Deepwater Horizon oil spill

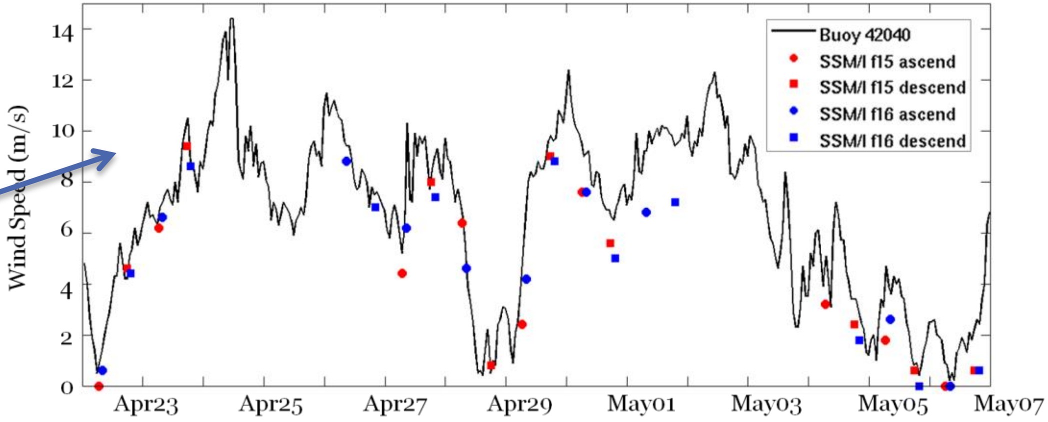

- Radiometer wind retrievals are affected by oil because some of the assumptions of the retrieval algorithm fail due to altered surface emissivity and the dielectric constant
- The oil slick introduces a wind speed bias into gridded products (CCMP and COAMPS) through compromised radiometer wind speed retrievals and reduced surface roughness

- The wind speed bias has a positive peak (~1.5 m/s) over the oil slick location, showing that CCMP winds > COAMPS on average
- The wind vector difference highlights substantial changes in the v-comp of the wind
- CCMP winds have better agreement with NDBC data in the oil affected regions

Task 3: Summary, Validation of COAMPS

- In general, good agreement between COAMPS and CCMP winds
- The magnitudes, timing and features of wind fields are well captured
- The frontal structure is similar (but not exact)
- The low wind speed areas behind the front are stronger in CCMP
- The oil slick may introduce a wind speed bias into gridded products such as CCMP and COAMPS through compromised radiometer wind speed retrievals and reduced surface roughness
- CCMP wind speeds are in better agreement with NDBC buoy wind speeds than COAMPS within the oil slick.
- COAMPS winds have noticeable negative bias (~1.5 m/s) in wind speeds over the oil slick compared to the CCMP and NDBC data

Task 3: Validation Methodologies for Surface Oil Drift Models and Quantitative Comparison Techniques for Spatial Patterns

Considered Metrics:

1) **Absolute Deviation** (absolute difference of the areas inside the contours)
2) **RMSD**
3) **Mean Displacement (MD)**
4) **Hausdorff Distance (HD)**
5) **Modified Hausdorff Distance (MHD)**

Root Mean Square Deviation

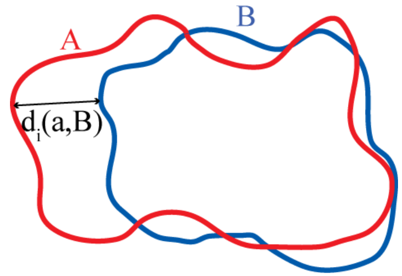

$$RMSD = \sqrt{\frac{\sum_{i=1}^{n}\left[d_i(A,B)\right]^2}{n}}$$

Mean Displacement

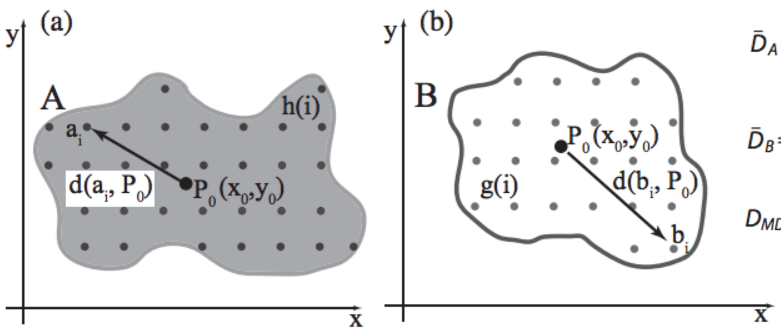

$$\bar{D}_A = \frac{1}{n}\sum_{i=1}^{n} h_i\, d(a_i, P_0),$$

$$\bar{D}_B = \frac{1}{m}\sum_{i=1}^{m} g_i\, d(b_i, P_0),$$

$$D_{MD3D}(A,B) = |\bar{D}_A - \bar{D}_B|,$$

Modified Hausdorff Distance

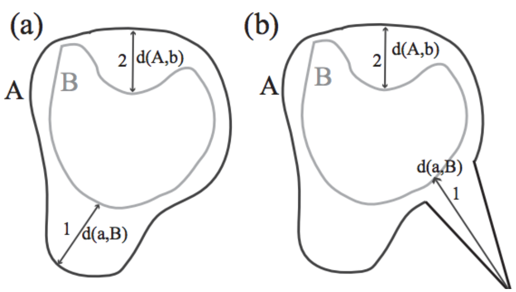

$$d_{MH}(A,B) = \max\left\{\frac{1}{|A|}\sum_{a\in A} d(a,B), \frac{1}{|B|}\sum_{b\in B} d(A,b)\right\}$$

where $d(a,B) = \min_{b\in B} d(a,b)$ and similarly for $d(A,b)$.

All metrics were analyzed and subjected to sensitivity and robustness tests. The study has been published in ***Dukhovskoy et al., 2015***.

Examples of application of MHD to geophysical fields are given in Dukhovskoy et al., 2015; Hiester et al., 2016;

Task 3: Summary, Validation Metrics

- Several metrics have been considered for a quantitative skill assessment of oil drift models (Mean Displacement, Weighted Mean Displacement, Hausdorff Distance, Modified Hausdorff Distance):
  - ✓ All metrics demonstrate the ability to identify differences in the shape of the oil spill and oil fraction coverage among the model experiments.
  - ✓ The RMSD rankings often are not consistent with other validation metrics. It also has high sensitivity to noise.
  - ✓ In the considered cases, the rotation and translation of the oil fields were negligibly small. Thus the Mean Displacement and Weighted Mean Displacement metrics agreed well with the topological metrics (HD and MHD).
  - ✓ The Mean Displacement method cannot penalize differences in the shapes' rotation or translation relative to each other. Not very robust to noise.
  - ✓ Skill metrics are somewhat sensitive to the choice of a contour that bounds compared fields.
- **The skill metric based on the Modified Hausdorff Distance is deemed to be the most appropriate for current study**
- The MHD metric is employed as an objective measure for the proximity of the numerical solution to observations or other control field. Low MHD score indicates good resemblance of the simulated oil spill to the control field.

Task 3: COAPS Surface Oil Drift Model

Realistic application of the MHD to the surface oil model evaluation and adjustment is demonstrated for the sensitivity runs with a surface oil drift model Each particle represents some volume of oil (estimated from the number of particles released per time step)

Surface oil drift model: Oil is simulated as Lagrangian particles advected by ocean currents, winds, and (optionally) waves

- Surface currents: 1/25° Gulf of Mexico HYCOM Analysis/Reanalysis
- Winds: CFSR, CCMP
- Wind drift parameterization (options):
  - ✓ 3.5% of the wind speed
  - ✓ Wind-dependent wind coefficient or user-specified constant value (e.g., 20° to the right of the wind vector)
- Laplacian diffusion of oil particles is parameterized as a random walk
- Half-life: Oil particles are removed randomly based on a prescribed half-life

Task 3: Testing MHD: Sensitivity Oil Model Experiments with Varying Parameters

MHD scores (vertical axis) from the sensitivity experiments

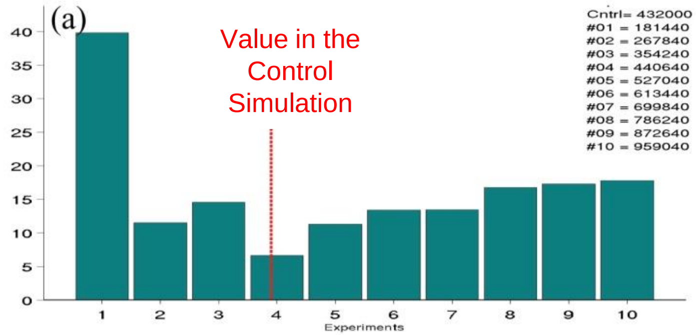

The MHD-based ranking of the simulations correctly identifies the case with the parameter value close to the control run

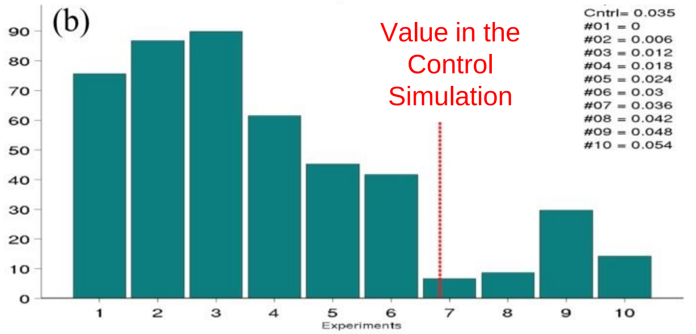

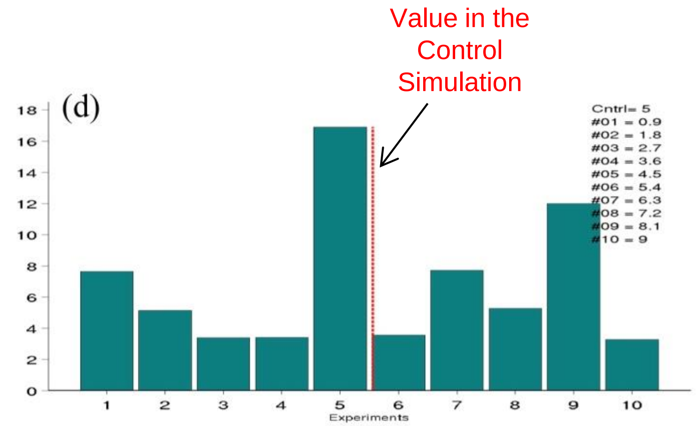

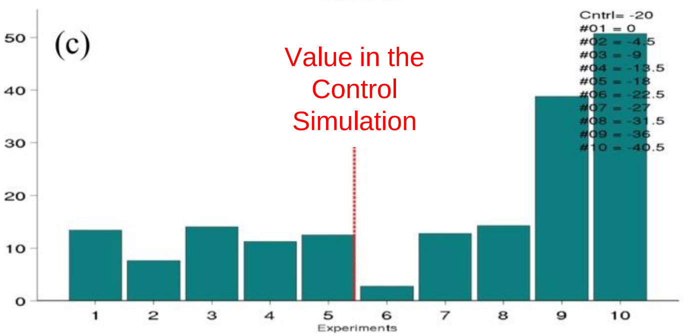

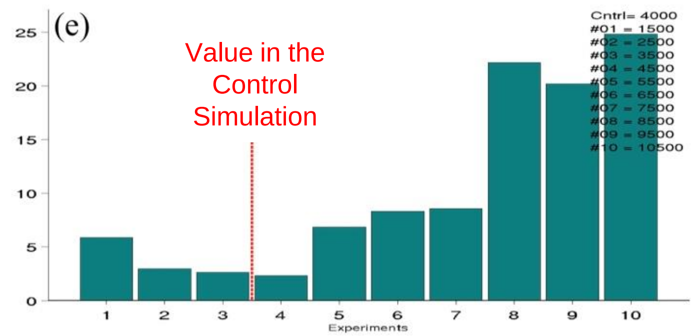

Task 3: Estimation of Half-life from SAR Observations and Oil Drift Model by Minimizing MHD Score

The MHD technique is employed to estimate half-life of surface oil particles from SAR observations by running sensitivity experiments with the oil drift model

Time-integrated SAR/TCNNA surface oil volume (m^3/km^2), May 23, 2010, 00Z.

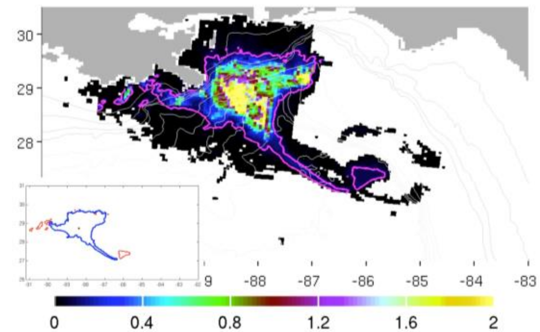

Contours of the time-integrated surface oil volume (0.09 m^3/km^2), May 23, 2010, 00Z from the simulations with varying half-life and SAR

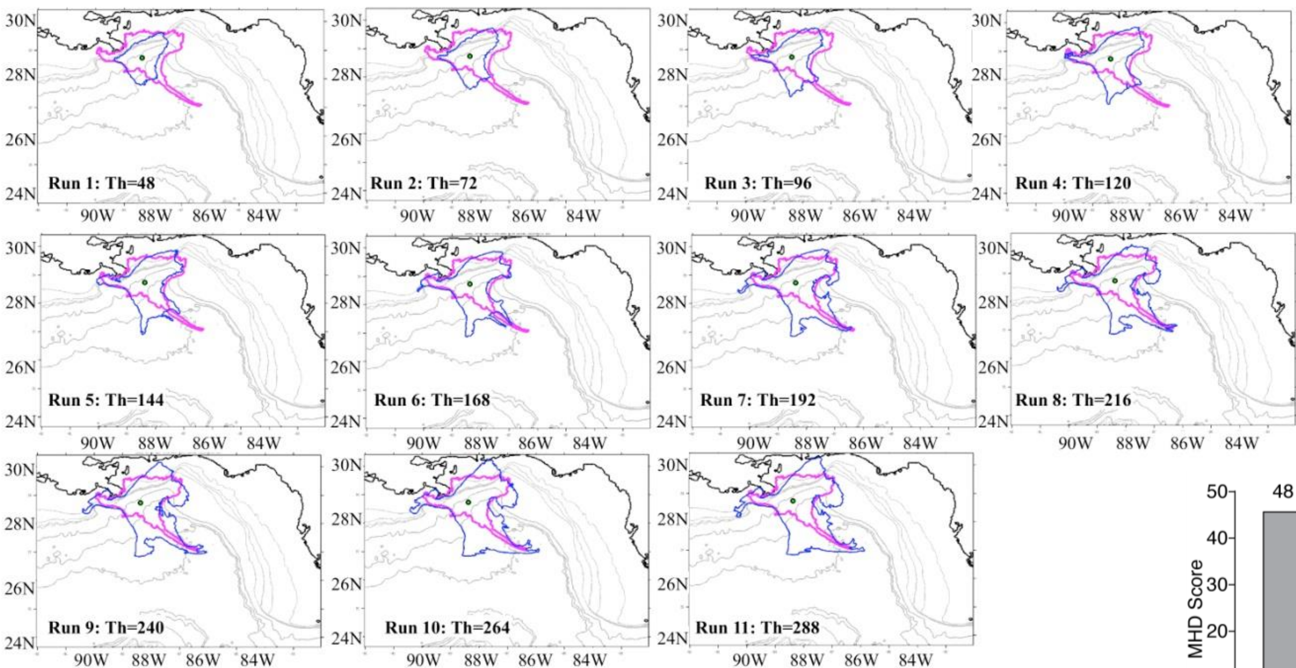

Skill metric scores for surface oil volume from the simulations with varying half-life parameter and SAR/TCNNA data.

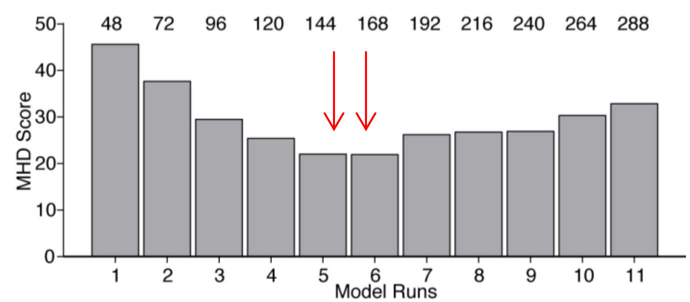

Task 4: Effects of Wind Forcing on Oil Drift

Oil drift is estimated as the vector sum of the surface drift component due to wind (W) and the surface current component (U)

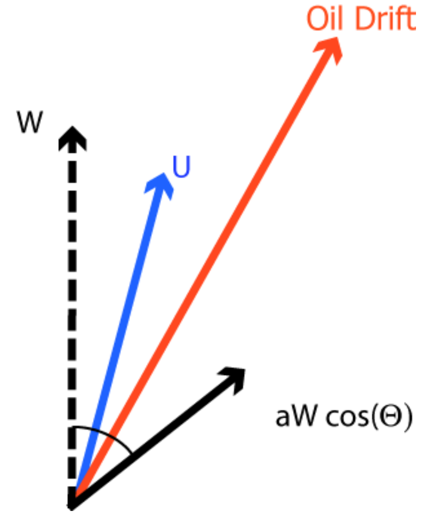

Surface drift component due to wind (W):

$$aW\cos(\theta)$$

wind factor (<5%)

deflection angle

Wind deflection angles as a function of wind speed

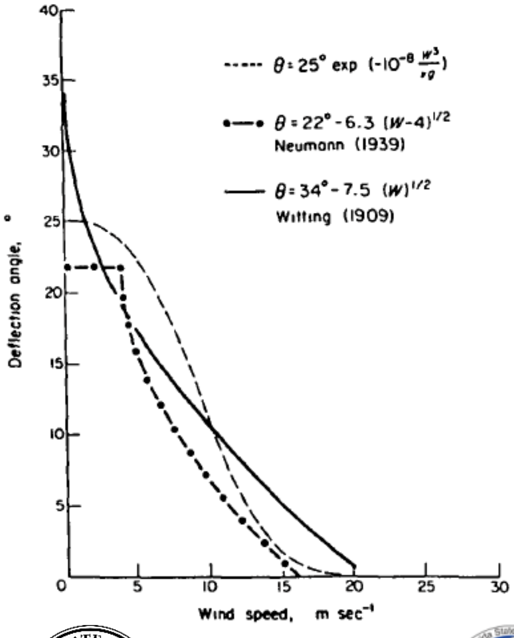

Deflection angle form *Samuels et al.* (1982)

$$\theta = 25°\exp\left(-10^{-8} W^{3}/\nu g\right)$$

- **Numerical experiments with the surface oil drift model indicate high sensitivity of the oil transport to the wind factor.**

- **Winds play important role in transporting oil towards the coast.**

Surface Oil Drift Model Hindcasts with Varying Wind Coefficient

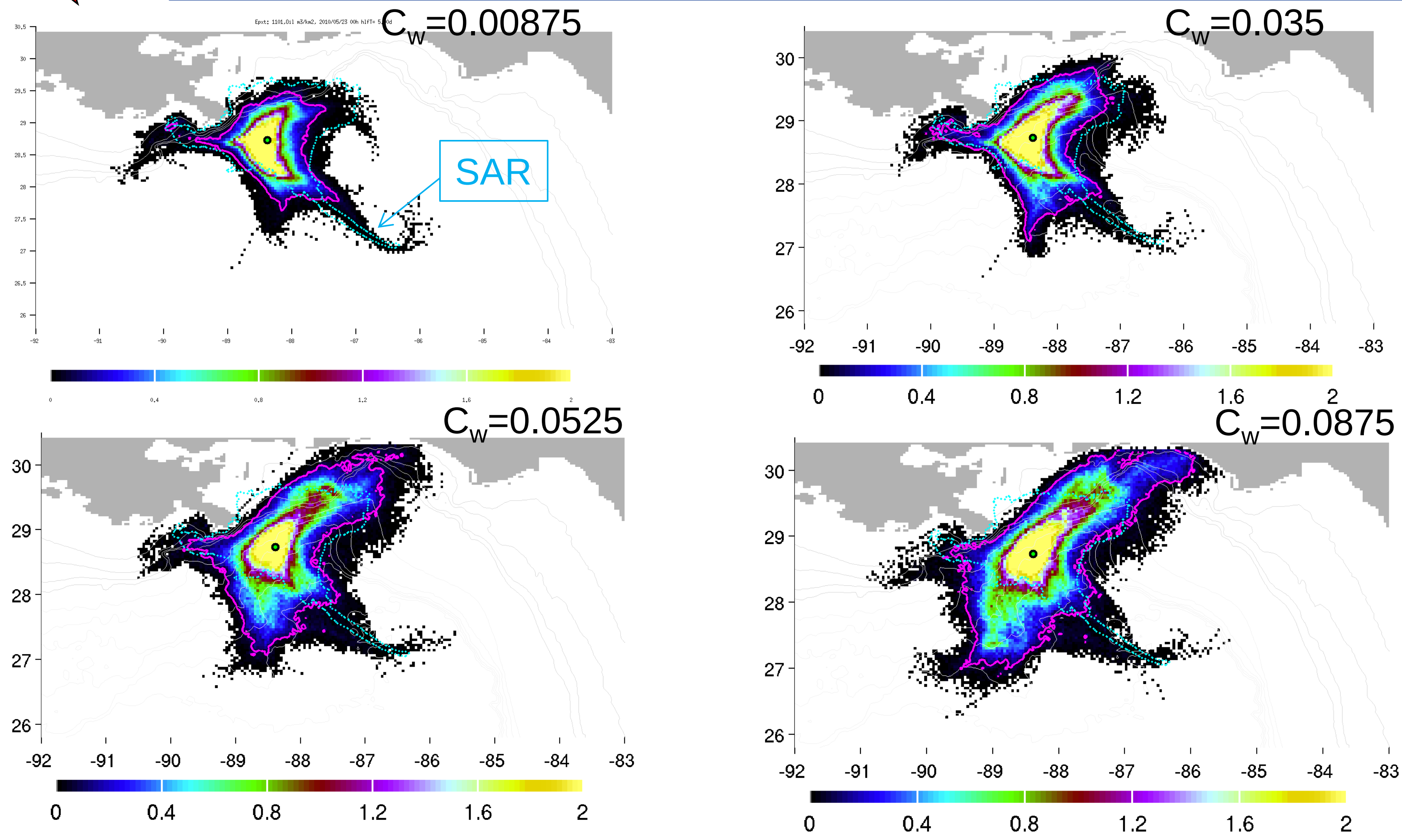

Task 4: “Surface Current” in a Model

Vertical layers in HYCOM GOMl0.04

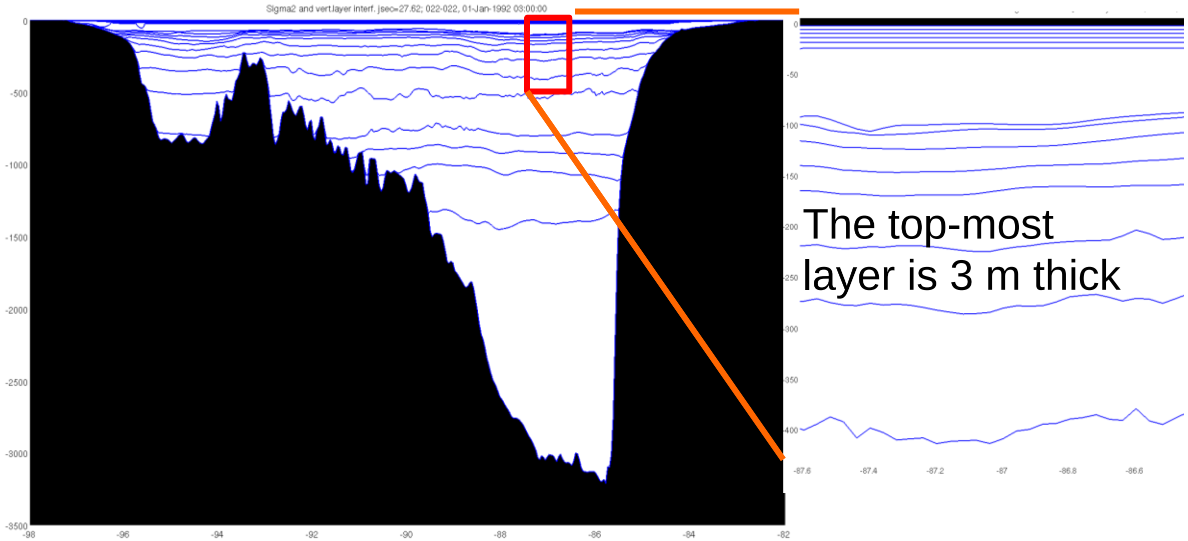

Approximation of the vertical temperature structure in a model

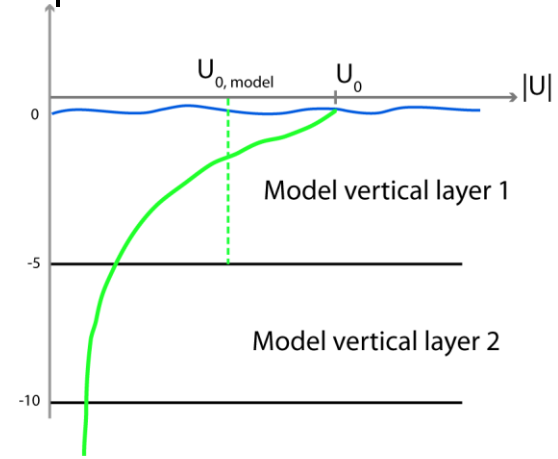

- Ocean “surface” currents from hydrodynamic models may be represented by very different depth-averaged velocity fields from the top-most layer. Depending on vertical grid and mixing parameterization in the surface layer velocity model, the accuracy of such an approximation may vary substantially across the models.
- Presumably, the hydrodynamic models with higher near-surface discretization and better physics would have a closer approximation of the true surface current. Thus, oil drift models forced with these surface currents may need reduced wind factor.
- Numerical sensitivity experiments with different forcing fields demonstrate that the optimal set of wind parameters that would fit all oil drift models cannot be derived. The set of wind parameters should be derived for an individual surface oil model depending on the surface current forcing fields.

Task 4: Modifications to Air/Sea Interaction

Oil dampens the roughness of the surface

- Capillary waves and wind waves were not observed for surface stresses typical of wind < ~8m^{s-1}.
- Highly damped at greater wind speeds

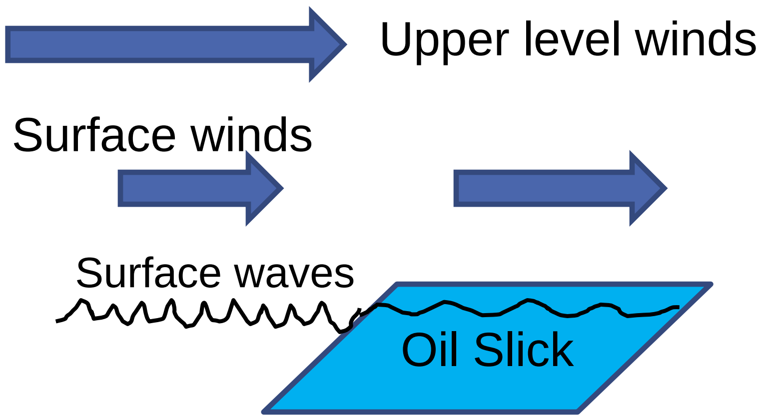

Oil causes

- Lower surface stress and greater surface winds
- A different balance between wind, roughness, and stress
- Weaker ocean Ekman transport
- Highly reduced latent heat flux from water (more from hydrocarbons)
- Greater near surface temperatures → Stronger stratification
- Modification of waves
- Damping of capillary waves and wind waves
- Allows swell (long waves generated from distant winds) to propagate

Task 5: Goals and Objectives

The goal of this part of the project is to investigate the possible existence of barriers to surface oil transport and whether they may be inferred from readily obtainable observational data.

Specific Objectives:

1. Identify oceanographic features that may serve as barriers (or constraints) to surface oil transport .
2. Analyze the transport of oil across boundaries inferred from SSH, surface salinity, temperature or velocity fields.
3. Determine the critical strengths of any such boundaries for limiting cross-barrier oil transport.

Task 5: Boundaries Inferred from Instantaneous Oceanographic Fields

- A **material boundary** separates different bodies of fluids – the boundary always marks the same fluid material as the fluid **evolves in time**.
- **Key Point:** Material boundaries are determined by analysis of the **time-dependent** flow field.
- In a slowly evolving flow field, locations of dominant material boundaries may possibly be approximated by features (fronts) in instantaneous fields.
- Should a readily-observable oceanographic field serve to approximately identify material boundaries, such a finding may aid in prediction of surface oil drift.

Task 5: Observations of Oceanic Fields

- Observations of (nearly) instantaneous fields of oceanographic variables are obtained only by satellite observations (in situ observations are too sparse to resolve mesoscale features).
- Radiometric sensors observe fields of surface temperature, surface color, and surface salinity (though presently lacking sufficient accuracy and resolution for these purposes).
  - ✓ Radiometric observations are heavily influenced by surface oil so inference of boundaries from these observations during an oil spill may be of limited practical use.
- Active microwave altimeters can detect SSH, but only at nadir (along-track observations).
  - ✓ SSH are sparse in time (10-35 days) and space (10-100km) cross-track spacing.
  - ✓ Statistical (gridding) or dynamical (assimilation into ocean models) methods are required to construct approximations of eddy-resolving SSH fields.

Task 5: Surface Oil Transport and Boundaries Inferred from SSH

- Material boundaries may approximately align with strong surface currents along fronts in a slowly-evolving ocean.
- SSH fronts indicate regions of strong geostrophic currents. Surface currents may have substantial ageostrophic components and deviate substantially from currents inferred from SSH.
- SSH fields from a data assimilating numerical model – The NRL HYCOM Gulf of Mexico Nowcast/Forecast model (hycom.org expt. 31.0) – are analyzed in conjunction with SAR TCNNA-derived surface oil coverage for the time period corresponding to the "tiger tail" formation (when oil was entrained into the Loop Current) in early-Mid May 2010.

Task 5: Boundaries Inferred from SSH

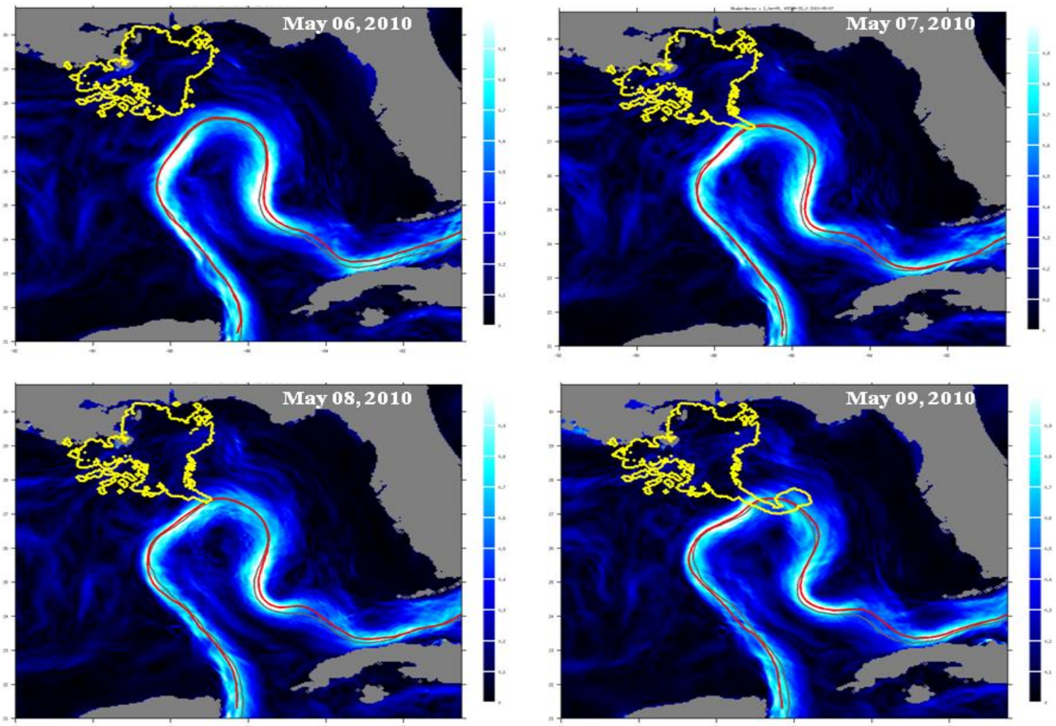

SSH gradient and Loop Current position. The core of the Loop Current is approximated by the 17 cm SSH anomaly contour (following Leben, 2005) and by a Kalman Filtering technique that adjusts the position toward the SSH gradient maximum (Dukhovskoy et al., 2015).

Surface oil determined by SAR-TCNNA is outlined in yellow.

- During the tiger tail formation, oil drifted from the main slick toward the Loop Current. Oil can be seen crossing the Loop Current front (but there is uncertainty in the exact front location due to sparse altimeter observations).
- There is no barrier here to oil entering the Loop Current in which rapid transport over long distance could occur under conditions of slow oil degradation. Oil might be inhibited from crossing the Loop Current to the interior bulge where it would be largely retained.

Task 5: Surface Oil transport and Instantaneous Surface Velocity Fields

- Surface velocity can be approximated from SSH fields by explicitly adding ageostrophic components to geostrophic currents inferred from statistically gridded SSH (e.g., the OSCAR surface current product – not to be confused with the OSCAR oil model), or dynamically from an atmosphere-forced ocean model that assimilates satellite SSH (e.g., HYCOM).
- Oil transport during the tiger tail formation time period is analyzed with two diagnostics derived from instantaneous velocity fields obtained from HYCOM: the Okubo-Weiss parameter and surface relative vorticity.

Task 5: Okubo-Weiss Parameter

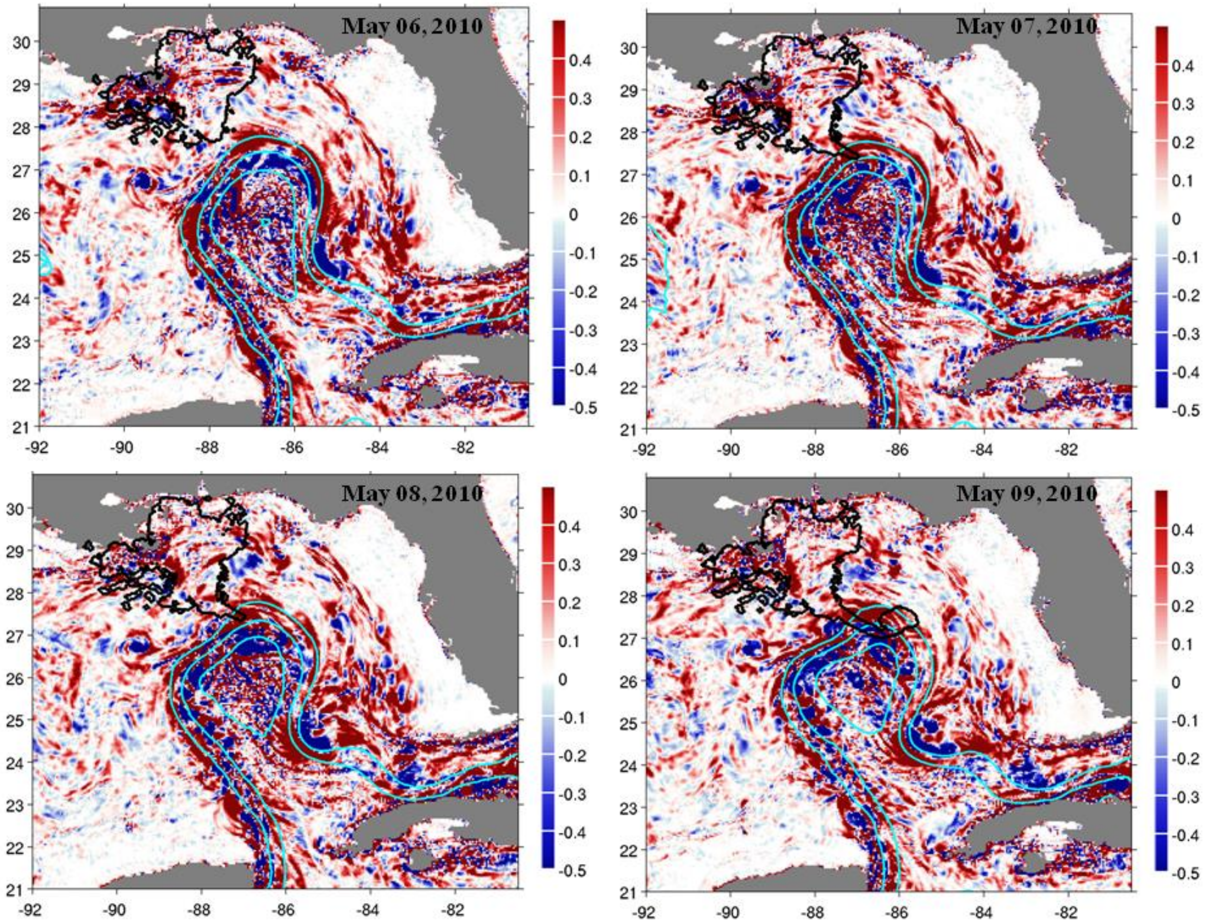

Okubo-Weiss parameter *is derived from deformation and relative rotation in the surface velocity field. Strong negative values may indicate eddies.*

Surface oil determined by SAR-TCNNA is outlined in black.

- The Okubo-Weiss parameter produces a very noisy field. No structures in the field appear to be related to movement of the surface oil.

Task 5: Surface Relative Vorticity

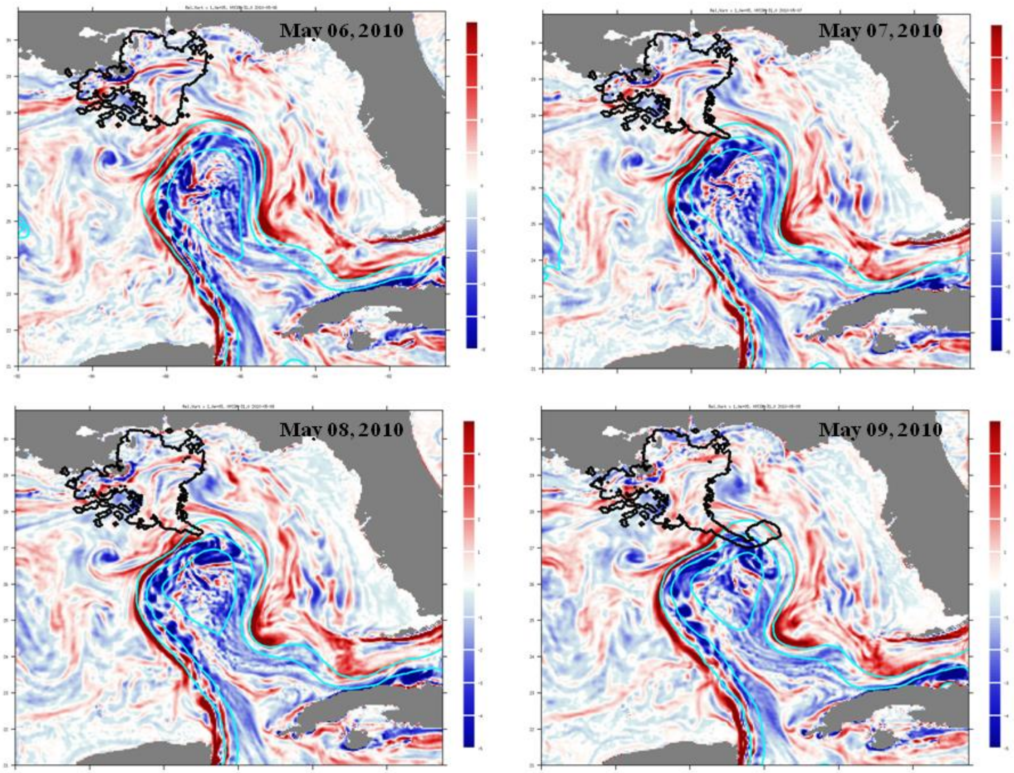

Surface relative vorticity.

Surface oil determined by SAR-TCNNA is outlined in black.

- Surface relative vorticity more clearly highlights jets, which have a characteristic rapid change in sign of the vorticity on either side of the core of the jet. The Loop Current is well-defined.
- The tiger tail enters and crosses the core of the jet as inferred from relative vorticity.
- There are no obvious structures in the vorticity field along the observed transport pathway of the tiger tail. Such structures might simply not exist or not be evident due to uncertainties in the surface currents from the data assimilative model.

Task 5: Lagrangian Coherent Structures and Surface Oil Transport

- **Lagrangian Coherent Structures (LCSs)** are material boundaries.
- LCS positions are determined through analysis of the time-evolving flow field over some finite time interval.
- LCSs are ridges in the **Finite Time Lyapunov Exponent (FTLE)** field, which characterizes the rate of stretching of neighboring trajectories.
  - ✓ LCSs determined from FTLE fields from forward-in-time trajectories are repelling.
  - ✓ LCSs determined from FTLE fields from backward-in-time trajectories are attracting.
- **LCSs evolve in time.** A location on one side of an LCS may at a later time be on the other side of the LCS (and LCSs continually form and disappear in an unstable flow field).

Task 5: Lagrangian Coherent Structures and Surface Oil Transport

Surface oil transport and relationships to LCSs are studied using a simple surface oil drift model driven by the NRL HYCOM Gulf of Mexico Reanalysis (expt 50.1).

- This simulation has improved representation of river plumes allowing investigation of oil transport and salinity gradients
- The time composite of simulated oil coverage agrees qualitatively well with SAR TCNNA time composites
- The tiger tail feature forms in this simulation, but a couple of weeks later than observations.

Model

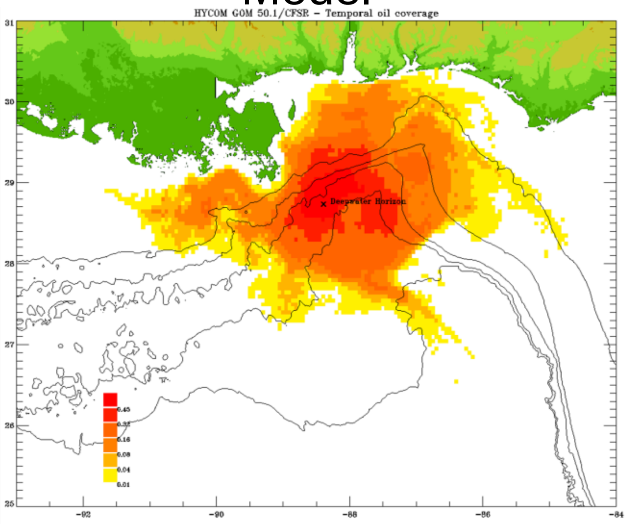

SAR-TCNNA

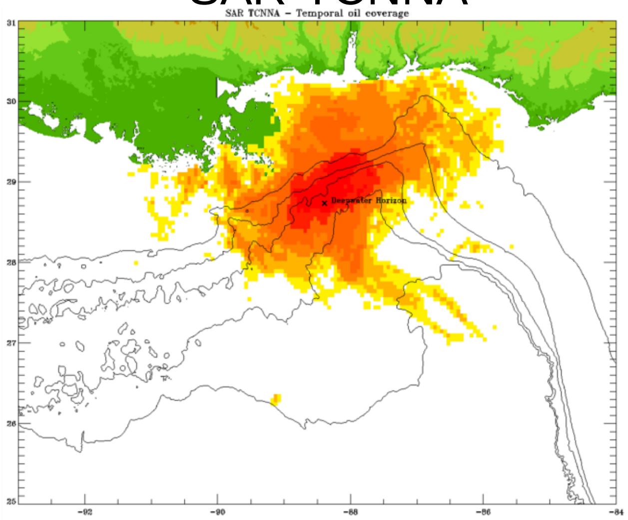

Fraction of time period (24 April – 14 July 2010) that each .05° x .05° bin had oil present

Task 5: Example of LCSs from an FTLE Field

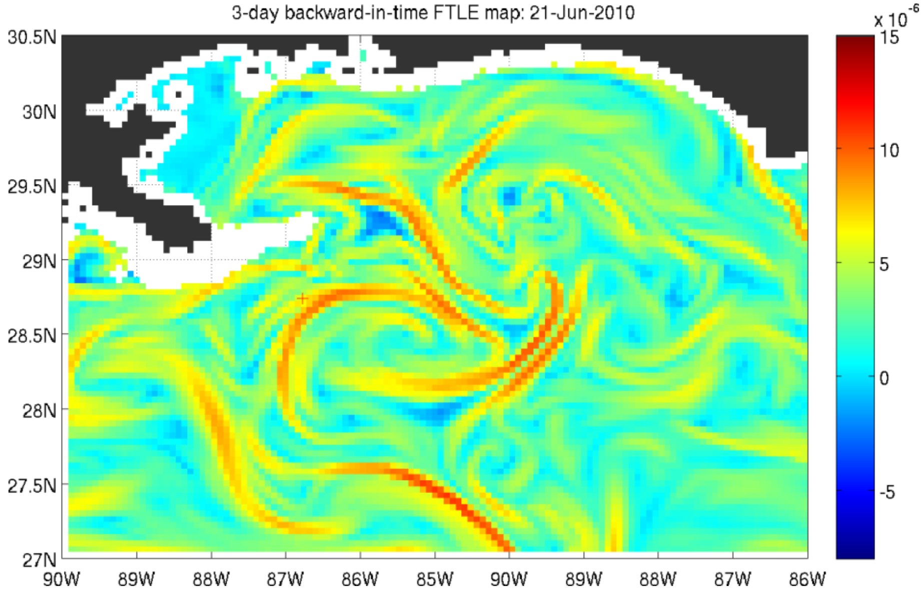

Backward-in-time FTLE field computed from HYCOM surface velocity data 18-21 June 2010.

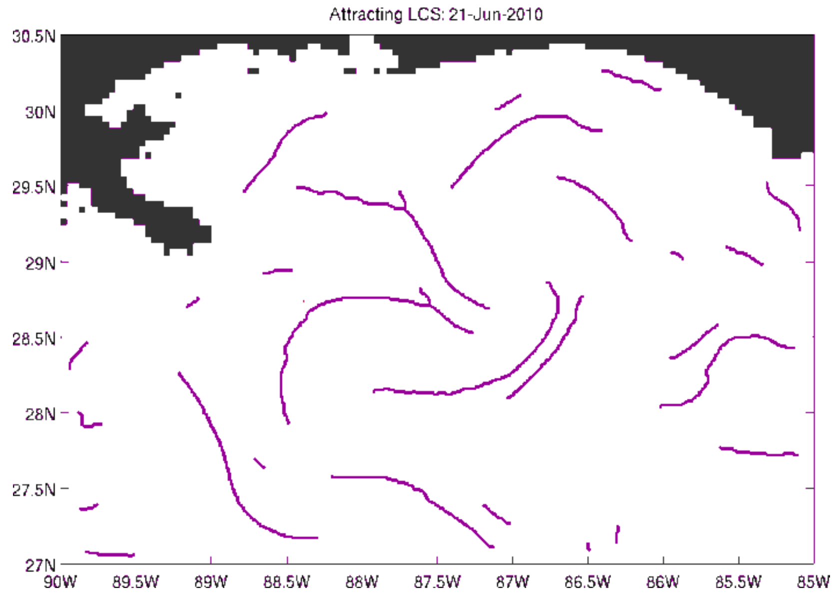

Attracting LCSs corresponding to the most dominant ridges in the FTLE field.

FLORIDA STATE UNIVERSITY 1851

COAPS

USF UNIVERSITY OF SOUTH FLORIDA

SINTEF

Task 5: LCS and SSH

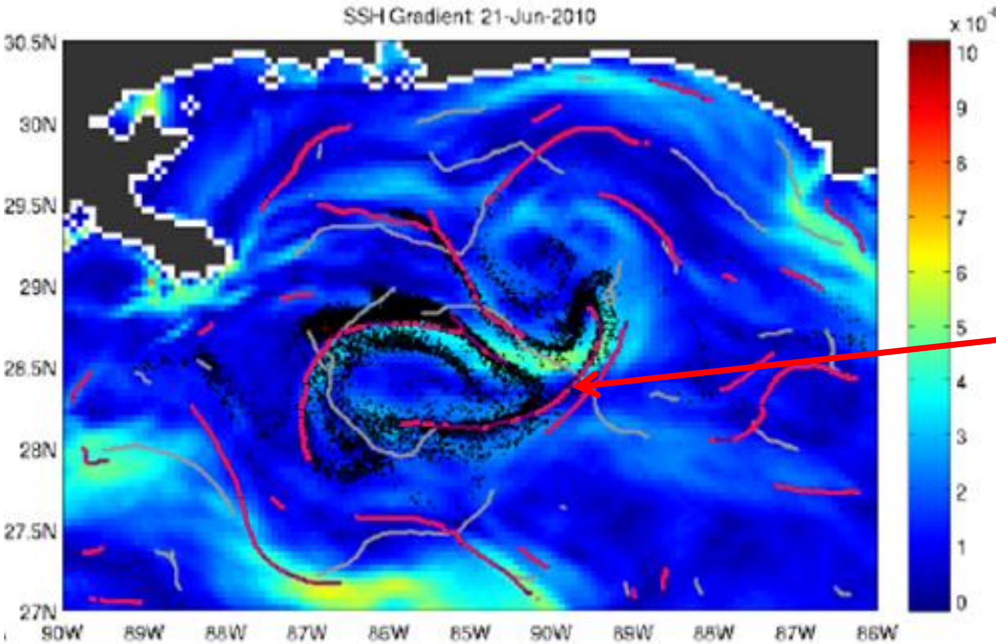

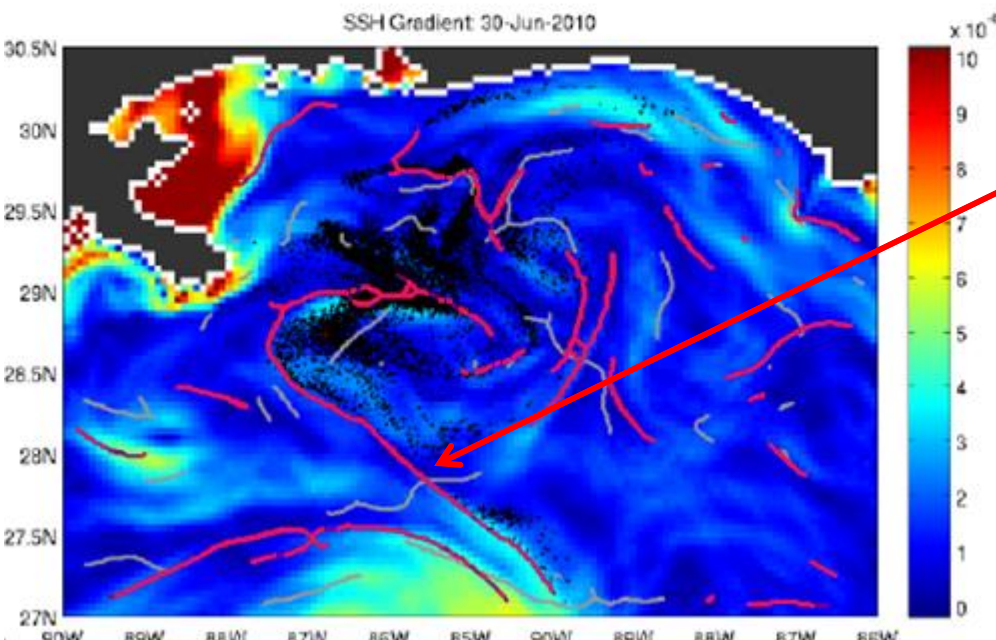

SSH Gradient and LCSs

(purple – attracting, gray – repelling)

Oil (simulated oil Lagrangian elements shown in black) tends to collect and be transported along attracting LCSs.

LCSs are prevalent near the Loop Current, but are not aligned with instantaneous SSH gradients.

An LCS connecting the region of the main body of oil to the Loop Current forms a conduit for oil to be transported to the LC region.

(see Olacoaga and Heller PNAS 2012)

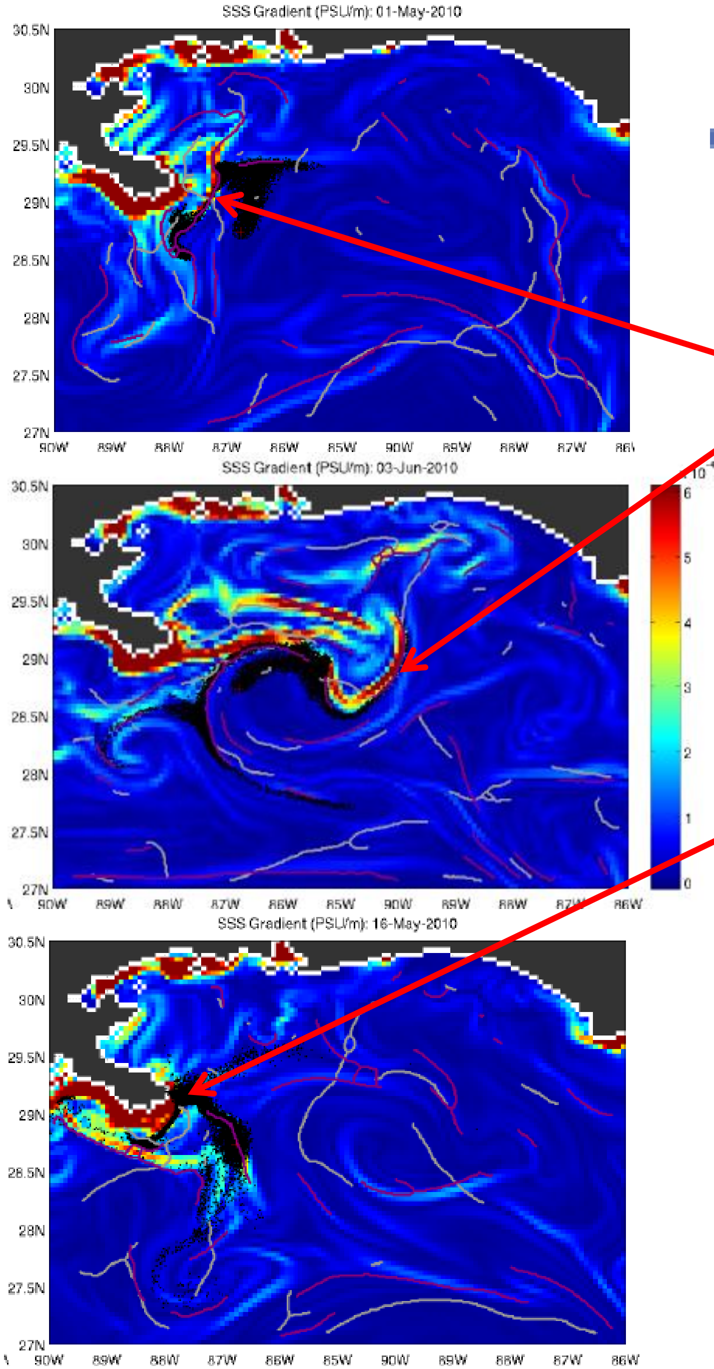

Task 5: LCS and Surface Salinity

Surface Salinity Gradient and LCSs
(purple – attracting, gray – repelling)

Oil converges along strong surface salinity gradients.

Attracting LCSs are aligned with strong gradients – likely due to buoyancy-driven currents.

These structures strongly constrain oil transport, serving as near-barriers, but at times oil can cross these zones of strong salinity gradients (hence beaching of oil along the MS river Delta).

(see Kourafalou and Androulidakis JGR 2013)

Task 5: Main Points

- Material boundaries are defined through analysis of the time-evolving flow field.
- Attracting LCSs determined from ridges in backward-in-time FTLE fields computed from time-evolving surface velocity fields highlight preferential pathways for oil transport.
- LCSs (or any constraints to surface oil transport) are not readily apparent from observed SSH or derived geostrophic velocity fields.
- LCSs are useful analysis tools, but application to forecasting requires forecasts of currents from a hydrodynamic model. It would likely be more straightforward to simply run an oil drift model than computing FTLE fields and deriving LCSs.
- Strong surface salinity gradients seem to be significant constraints (but not impermeable barriers) to surface oil transport. Previous satellite observations of salinity (Aquarius) are not high enough resolution for these purposes, but the new SMAP mission should be investigated for potential utility to oil spill prediction.

Recommendations for Future Research

- Further investigation of the dynamics of near-surface velocity structure using newly available observational techniques leading to new parameterizations.
- Improve parameterization of wave effects on oil transport considering directional wave spectrum.
- Extend weathering and transport oil prediction capabilities for cold (temperate latitude winter or Arctic) conditions.
- Higher resolution salinity data from the new SMAP (Soil Moisture Active Passive) mission should be investigated for potential utility to oil spill prediction given the correspondence of salinity gradients and attracting LCSs.
- Improve technology for characterizing oil, including measuring oil thickness and volume, in the laboratory and the field and using remotely sensed data.
- Improve understanding of emulsification processes and how emulsified oil drifts differently from thin oil.